Augmentation Techniques for Satellite-Based Maritime Navigation in the Baltic Sea

Michelle Koivisto

School of Electrical Engineering

Thesis submitted for examination for the degree of Master of Science in Technology.

Espoo 30.1.2019

Supervisor

Prof. Jaan Praks

Advisor

Dr. Mohammad Zahidul H. Bhuiyan

Aalto University
School of Electrical
Engineering

Aalto University
School of Electrical Engineering

Aalto University, P.O. BOX 11000, 00076 AALTO
www.aalto.fi
Abstract of the master's thesis

Author Michelle Koivisto

Title Augmentation Techniques for Satellite-Based Maritime Navigation in the Baltic Sea

Degree programme Master's Programme in Electronics and Nanotechnology

Major Space Science and Technology **Code of major** ELEC3039

Supervisor Prof. Jaan Praks

Advisor Dr. Mohammad Zahidul H. Bhuiyan

Date 30.1.2019 **Number of pages** 71 **Language** English

Abstract

Maritime navigation in the Baltic Sea is challenging, even for the experienced navigator. Anomalies in the sea level caused by postglacial land uplift and the irregular motion of the Earth's rotation around its own axis are only part of the many challenges faced by the navigator. Low elevation angles and visibility of Global Navigation Satellite System (GNSS) satellites are other challenges at northern latitudes. Techniques to overcome these challenges are possible through different satellite-based augmentation techniques. The Differential Global Positioning System (DGPS) provided by the Finnish Transport Infrastructure Agency (formerly Liikennevirasto, LiVi) and the Satellite-Based Augmentation System (SBAS) offered by the European Geostationary Navigation Overlay Service (EGNOS) Data Access Service (EDAS) are evaluated in this thesis. GNSS data is analysed from two days of the FAMOS project's week-long test campaign in the Baltic Sea on the research vessel Aranda.

Results show that the availability and accuracy of EGNOS corrections decrease on day 2 when the vessel is in the north Baltic Sea regions close to the edge of the EGNOS coverage area. EGNOS performs significantly better on day 5 when the vessel is travelling at more southern latitudes. On this day, EGNOS offers the largest improvement to GPS compared to LiVi DGPS. LiVi corrections show almost the same level of performance on both days of the test campaign, because of the densely located DGPS stations by the Finnish coastline. On day 5 the Åland islands are located between the vessel and the nearest LiVi DGPS station, causing the horizontal accuracy to slightly decrease compared to day 2. An alternative Differential GNSS (DGNSS) augmentation technique is presented in this thesis called the State Space Representation (SSR) correction model from the Finnish Permanent GNSS Network FinnRef. This technique provides an accurate and reliable augmentation of GPS reaching closely to the performance level of LiVi on day 2.

This thesis presents a performance analysis of satellite-based augmentation techniques in a real-life situation for a vessel travelling in the Baltic Sea. The analysis confirms that maritime navigation at northern latitudes becomes more reliable, accurate and precise when EGNOS, LiVi or SSR corrections are applied by the navigator.

Keywords Maritime, navigation, Baltic Sea, GPS, GNSS, SBAS, DGPS, EGNOS

Aalto University
School of Electrical Engineering

Aalto-universitetet, PB 11000, 00076 AALTO
www.aalto.fi
Sammandrag av diplomarbetet

Författare Michelle Koivisto

Titel Hjälpsystem för satellitnavigering inom sjöfarten i Östersjön

Utbildningsprogram Master's Programme in Electronics and Nanotechnology

Huvudämne Space Science and Technology **Huvudämnets kod** ELEC3039

Övervakare Prof. Jaan Praks

Handledare TkD Mohammad Zahidul H. Bhuiyan

Datum 30.1.2019 **Sidantal** 71 **Språk** Engelska

Sammandrag

Sjöfartsnavigering i Östersjön kan vara en krävande uppgift, även för en erfaren navigatör. Utmaningarna i Östersjön är bland annat höjdskillnader i havsnivån på grund av postglacial landhöjning och jordens oregelbundna rotation kring sin egen axel. Satellitnavigering på norra breddgrader är också utmanande på grund av (GNSS) Global Navigation Satellite System-satelliternas låga höjdvinklar och låga synlighet. Olika tekniker för att övervinna dessa utmaningar är olika hjälpsystem som förbättrar (GPS) Global Positioning System-signalen. (DGPS) Differential Global Positioning System-servicen från Trafikledsverket i Finland (tidigare Liikennevirasto, LiVi) och (SBAS) Satellite-Based Augmentation System-servicen som European Geostationary Navigation Overlay Service (EGNOS) Data Access Service (EDAS) erbjuder, analyseras i den här avhandlingen. Utvärderingen består av GNSS-data som samlades under två dagar från FAMOS-projektets veckolånga test i Östersjön på forskningsfartyget Aranda.

Forskningsresultatet visar att tillgängligheten och noggrannheten av EGNOS minskar under den andra testdagen då Aranda befinner sig på norra breddgrader nära gränserna för EGNOS täckningsområde. EGNOS förbättrar GPS märkbart på den femte testdagen då Aranda befinner sig på mer sydliga breddgrader. På den femte testdagen förbättrar EGNOS GPS-signalen allra mest jämfört med LiVi-resultatet. LiVi erbjuder liknande noggrannhet och tillgänglighet under de två testdagarna, på grund av de tätt belägna DGPS-stationerna vid den finska kusten. På den femte testdagen är Åland beläget mellan Aranda-fartyget och den närmaste LiVi DGPS-stationen, vilket orsakar att noggrannheten i den vågräta riktningen minskar i jämförelse med den andra testdagen. En alternativ Differential GNSS (DGNSS) förbättringsteknik för GPS presenteras i den här avhandlingen, nämligen (SSR) State Space Representation-korrigeringsmodellen från Finlands permanenta GNSS-nätverk FinnRef. SSR erbjuder en noggrann och tillförlitlig förbättring för GPS-signalen och presterade nästan lika väl som LiVi-hjälpsystemet på den andra testdagen.

Den här avhandlingen presenterar en noggrannhetsanalys av olika hjälpsystem för satellitnavigering i en verklig situation för ett fartyg som färdas på Östersjön. Analysen bekräftar att sjöfartsnavigering på norra breddgrader är mer tillförlitlig, noggrann och exakt när navigatören använder sig av EGNOS-, LiVi- eller SSR-hjälpsystem.

Nyckelord Sjöfartsnavigering, Östersjön, GPS, GNSS, SBAS, DGPS, EGNOS

Preface

I have written this thesis in the Department of Navigation and Positioning at the Finnish Geospatial Research Institute (FGI) at the National Land Survey of Finland (NLS). The data used in this thesis is part of the international FAMOS project coordinated by the Swedish Maritime Administration and co-financed by the European Union's Connecting Europe Facility (CEF). The satellite-based augmentation data was collected from the Differential Global Positioning System (DGPS) service provided by the Finnish Transport Infrastructure Agency (formerly Liikennevirasto, LiVi) and from the European Geostationary Navigation Overlay Service (EGNOS) Data Access Service (EDAS).

I want to thank my advisor Dr. Mohammad Zahidul H. Bhuiyan for his assistance and contribution to this thesis. I am also grateful for the help and guidance of my supervisor Prof. Jaan Praks. My grateful thanks are also extended to Prof. Sanna Kaasalainen for giving me the opportunity to complete my thesis in the Department of Navigation and Positioning at FGI. I want to express a special thank you to all my colleagues at FGI for the great work environment and encouragement throughout my thesis work. Assistance provided by Lic.Sc. Stefan Söderholm, Lic.Sc. Hannu Koivula, M.Sc. Mirjam Bilker-Koivula and M.Sc. Kaisu Heikonen were greatly appreciated.

Finally, I want to express my deepest gratitude to my family and friends, for always standing by my side and believing in me.

Espoo, 30.1.2019

Michelle Koivisto

Contents

Symbols and Abbreviations

Symbols

Latin Symbols

a	semimajor axis
c	speed of light in vacuum $\approx 3 \times 10^8$ [m/s]
e	eccentricity
$\mathrm{I_{i,corr}}$	ionospheric correction factor for the $\mathrm{i^{th}}$ SV
R_b	data rate
r	true range
T	true anomaly
T_b	bit period
$\mathrm{T_{i,corr}}$	tropospheric correction factor for the $\mathrm{i^{th}}$ SV
$\mathrm{T_{i,GD}}$	group delay differential for the $\mathrm{i^{th}}$ SV
T_s	system time
T_u	receiver time
$\mathrm{t_{i,current}}$	time of the $\mathrm{PRC_{i,current}}$ for the $\mathrm{i^{th}}$ SV
$\mathrm{t_{i,previous}}$	time of the $\mathrm{PRC_{i,previous}}$ for the $\mathrm{i^{th}}$ SV
$\mathrm{t_{rec}}$	time of the observable
t_u	time offset
x_j	j^{th} satellite's position in x-direction
x_u	receiver's position in x-direction
y_j	j^{th} satellite's position in y-direction
y_u	receiver's position in y-direction
z_j	j^{th} satellite's position in z-direction
z_u	receiver's position in z-direction

Greek Symbols

$\Delta_{\mathrm{i,tsv}}$	clock correction term for the $\mathrm{i^{th}}$ SV
ΔR_{error}	range error
ΔT_{error}	clock error
$\delta_{\mathrm{i,corr}}$	clock correction factor for the $\mathrm{i^{th}}$ SV
δt	time offset
$\delta\Delta_{\mathrm{i,tsv}}$	clock time error estimate for the $\mathrm{i^{th}}$ SV
ρ	pseudorange
Ω	right ascension of ascending node
ω	argument of perigee

Abbreviations

AFS	Atomic Frequency Standard
ATAFS	Advanced Technology Atomic Frequency Standard
BPSK	Binary Phase Shift Keying
C/A	Coarse/Acquisition
CDDS	Commercial Data Distribution Service
CDMA	Code Division Multiple Access
CEP	Circular Error Probable
CNAV	Civil Navigation Message
CPF	Central Processing Facilities
CQI	Correction Quality Indicator
DGNSS	Differential Global Navigation Satellite System
DGPS	Differential Global Positioning System
DSSS	Direct Sequence Spread Spectrum
ECEF	Earth-Centered, Earth-Fixed
EDAS	EGNOS Data Access Service
EGNOS	European Geostationary Navigation Overlay Service
ESA	European Space Agency
EWAN	EGNOS Wide Area Network
FGI	Finnish Geospatial Research Institute
FTIA	Finnish Transport Infrastructure Agency
FTP	File Transfer Protocol
GAGAN	GPS and GEO Augmented Navigation
GEO	Geostationary
GLONASS	Globalnaya Navigazionnaya Sputnikovaya Sistema
GNSS	Global Navigation Satellite System
GPS	Global Positioning System
HNSE	Horizontal Navigation System Error
IM	Integrity Monitor
IMO	International Maritime Organization
IMU	Inertial Measurement Unit
IOD	Issue of Data
ITU	International Telecommunication Union
LiVi	Liikennevirasto, since January 2019 Väylävirasto
MCC	Mission Control Centre
MCS	Master Control Station
MEO	Medium Earth Orbit
MMD	Mean Mission Duration
MSAS	Multi-functional Satellite Augmentation System
MSC	Maritime Safety Committee
MSK	Minimum Shift Keying
NCO	Numerically Controlled Oscillators
NCSR	Navigation, Communications and Search and Rescue
NLES	Navigation Land Earth Stations

Abbreviations

OS	Open Service
PNT	Position, Navigation and Timing
PPP	Precise Point Positioning
PPS	Precise Positioning Service
PR	Pseudorange
PRC	Pseudorange Correction
PRN	Pseudorandom Noise
QZSS	Quasi-Zenith Satellite System
RA	Right Ascension
RAFS	Rubidium Atomic Frequency Standard
RF	Radio Frequency
RHCP	Right Hand Circular Polarized
RIMS	Ranging Integrity Monitoring Stations
RINEX	Receiver Independent Exchange Format
RNS	Radio Navigation System
RR	Range Rate
RS	Reference Station
RRC	Range Rate Correction
RSIM	Reference Station/Integrity Monitor
RTCM	Radio Technical Commission for Maritime Services
RTK	Real-Time Kinematic
SA	Selective Availability
SBAS	Satellite-Based Augmentation System
SCREW	Satellite Residual Error for the Worst User Location
SDCM	System for Differential Corrections and Monitoring
SEP	Spherical Error Probable
SISNet	Signal in Space through the Internet
SNAS	Satellite Navigation Augmentation System
SoL	Safety of Life
SPS	Standard Positioning Service
SSR	State Space Representation
SV	Space Vehicle
SVN	Space Vehicle Number
TKS	Time Keeping System
TOW	Time Of Week
UDRE	User Differential Range Error
UERE	User Equivalent Range Error
UIVD	User Ionospheric Vertical Delay
UTC	Coordinated Universal Time
VCXO	Voltage Controlled Crystal Oscillator
VNSE	Vertical Navigation System Error
WAAS	Wide Area Augmentation System
WADGPS	Wide Area Differential Global Positioning System
WWRNS	World-Wide Radio Navigation System

1 Introduction

The heavy maritime traffic in the Baltic Sea urges for new technological solutions to make maritime navigation more efficient and safe. New techniques for safer and more accurate maritime navigation are developed at an increasing rate [1].

The Baltic Sea is a challenging region for efficient maritime navigation because of different effects causing anomalies in the sea level. Among these are postglacial land uplift, climatic sea level rise, winter sea level changes, pole tides and mean sea surface topography. The postglacial land uplift is the result of the thick ice cover which melted in the end of the Ice Age. The rebound effect of the crust causes land uplift. The melting of glaciers and sea temperature rise induce climatic sea level rise. Winter sea level changes occur due to seasonal changes and the largest changes occur in winter. Polar motion leads to pole tides which appear as anomalies in the sea level [2]. This motion is created by the Earth's rotational motion around its own axis. This centrifugal force is not constant and it generates anomalies in the sea level. Changes in this force vector perturb the oceans which then translates into anomalies in the sea level. Oceans strive towards their state of equilibrium when perturbed [3]. In the Baltic Sea the salinity of the water is inconsistent. This inconsistency changes the mean sea surface topography [2].

All of these effects, causing anomalies in the sea level, urge the technological community to come up with new ideas and solutions to navigate safely in the Baltic Sea. The person navigating the vessel needs to be experienced and aware of the anomalies in the sea level before taking the wheel. However, more often than not the people navigating vessels make mistakes which may have catastrophic consequences. These errors in maritime navigation are up to 60% caused by human. Accurate and reliable navigation solutions may prevent most of these accidents from happening. Both Differential Global Navigation Satellite System (DGNSS) and Satellite-Based Augmentation System (SBAS) are capable of providing robust Position, Navigation and Timing (PNT) data to vessels [1].

The International Maritime Organization (IMO) is an agency of the United Nations which is responsible for the safety and security of shipping. In addition, the IMO is also responsible for preventing maritime and atmospheric pollution by maritime vessels. All the standards used in the maritime sector for safety, security and environment are set by the IMO [4]. The operational requirements for Radio Navigation Systems (RNSs) are set by the IMO and the approved systems are part of the World-Wide RNS (WWRNS). Among GNSS signals that are components of the WWRNS are the Global Positioning System (GPS), the Globalnaya Navigazionnaya Sputnikovaya Sistema (GLONASS) and BeiDou. In addition, DGNSS is an IMO regulated augmentation system accepted as part of the WWRNS. SBAS is not yet part of the WWRNS and is therefore not regulated by the IMO [1]. In May 2012, the 90^{th} session of the IMO Maritime Safety Committee (MSC) initiated the requirement for advancing new "Performance Standards For Multi-System Shipborne Navigation Receivers" ([5], [6]). The Sub-Committee on Navigation, Communications and Search and Rescue (NCSR) endorsed this initiative in their 2^{nd} session in March 2015. This session required the MSC 95 in 2017 to authorize the development of

this initiative. The 4^{th} session of the NCSR in March 2017 accepted further work on new performance standards for multi-systems in maritime navigation ([5], [7], [8]). The initiative by IMO to achieve safer maritime navigation through the collection, distribution and presentation of maritime data electronically is called e-Navigation. This initiative may forward many advances in multi-systems in maritime applications such as DGNSS assisted with SBAS or Galileo as part of the WWRNS [1].

GPS, GLONASS or BeiDou used alone in critical maritime operations, e.g. navigating close to harbors, are not enough to safely perform these operations. Augmentation systems are necessary during these critical operations. As mentioned earlier, DGNSS is an augmentation system which is part of the WWRNS. DGNSS augments the GNSS signals and ensures the safe performance of maritime vessels during critical operations. DGNSS was first initiated because of Selective Availability (SA) which degraded the accuracy of the GPS signal. The SA was discontinued in May 2000, however DGNSS is still used for augmenting the GNSS signals in the maritime sector ([1], [9]).

This thesis contributes to navigation safety by developing and comparing satellite-based augmentation techniques in maritime navigation. The goal of this work is to investigate how well the DGPS and SBAS augmented techniques work in a real-life situation for a vessel travelling in the Baltic Sea, and to compare the accuracy of these techniques. The challenges faced in the Baltic Sea are solved through augmenting the GPS signal. Satellite-based augmentation techniques correct the errors of the GPS signal by providing a closer representation of atmospheric and satellite related effects for the signal. The more accurate corrections that these techniques are able to provide the more accurate and precise the navigation solution of the receiver becomes. This is important to achieve because of the heavy maritime traffic and the anomalies in the sea level of the Baltic Sea.

The data used in this thesis was collected from the test campaign in June 2017 as part of the international project FAMOS. This project is led by the Swedish Maritime Administration and it is co-financed by the European Union Connecting Europe Facility. The Finnish Geospatial Research Institute (FGI) at the National Land Survey of Finland (NLS) is a partner in this project. At FGI, the project is led by the Department of Geodesy and Geodynamics and the GNSS research is led by the Department of Navigation and Positioning. During the test campaign data was collected with different GNSS receivers on board the research vessel Aranda of the Finnish Environment Research Institute (SYKE) from the 5^{th}-10^{th} of June 2017. In this thesis, the GPS data collected from a professional-grade NovAtel receiver is augmented through the DGPS service of the Finnish Transport Infrastructure Agency (FTIA, formerly, Liikennevirasto, LiVi) and the SBAS service of the European Geostationary Navigation Overlay Service (EGNOS) Data Access Service (EDAS). The DGPS corrections from LiVi are obtained from the DGPS stations in Finland and the SBAS corrections are collected from the EDAS File Transfer Protocol (FTP) service which are broadcast from the Geostationary (GEO) satellites of EGNOS. An additional DGNSS augmentation technique is presented in this work, namely a State Space Representation (SSR) correction model from the Finnish Permanent GNSS Network FinnRef operated by FGI. In this thesis, the SSR correction model's

performance and capability to augment the GPS signal in the maritime sector are compared with respect to LiVi and EGNOS.

In addition to the challenges in the Baltic Sea, the area covered by the test campaign introduces some additional challenges in satellite navigation, e.g. low elevation angles and visibility of GNSS satellites. A low elevation angle of a satellite causes a weak signal strength and a low accuracy. The low visibility of satellites at northeastern latitudes in Europe leads to a decreased amount of corrections provided by satellite-based augmentation techniques such as EGNOS [10]. In addition, less satellites used in the navigation solution leads to a decrease in position accuracy. These limitations are examined further in this thesis when the data collected at two different latitude degrees are being compared with respect to each other.

Chapter 2 includes the background information of GPS, the GPS signal, the receiver position and the GPS errors. Chapter 3 gives an overview of DGPS and SBAS and how they augment the GPS signal. The FAMOS project, the test campaign and the software analysis tool are described in Chapter 4. The performance comparison of the augmentation techniques is provided in Chapter 5 including the additional augmentation technique SSR provided by FinnRef in Section 5.4. Chapter 5 contains also a summary of the performance comparison and Chapter 6 gives the conclusion of this thesis.

2 Satellite-Based Positioning

This chapter describes the three segments of GPS namely: the space, control and user segments. This is followed by a description of the GPS signal and the contents of the navigation message. The receiver position computation is explained and the fundamental equations for positioning are given in this chapter. Additionally, the GPS errors are characterized and described here.

2.1 Global Positioning System (GPS)

The GPS satellite-based RNS is owned by the United States (U.S.). Other GNSS systems in the world are Russia's GLONASS, China's BeiDou Navigation Satellite System, Europe's Galileo and Japan's Quasi-Zenith Satellite System (QZSS). This study includes a more detailed description about GPS and the GPS signal. GPS is threefold including a space segment, a control segment and a user segment. The space segment is the GPS Navstar satellites orbiting around Earth broadcasting the GPS signals to the user and control segments. The control segment controls and monitors the satellite health and the integrity of the signal. The orbital characteristics of the GPS satellites are managed by the control segment. The user segment is the GPS receiver itself which obtains the Radio Frequency (RF) signals for positioning ([11], pages 67-69).

2.1.1 Space Segment

The space segment of GPS consists of the Navstar satellite constellation. In May 2018 the GPS constellation included 32 operating Block II/IIA/IIR/IIR-M satellites [12]. The GPS constellation status obtained on May 9^{th} 2018 is shown in Figure 1 [13]. The figure shows the Space Vehicle Number (SVN) and the Pseudorandom Noise (PRN) of each GPS satellite in the first two columns. The third column in Figure 1 gives the launch date of each satellite and the fourth column lists the dates when the satellite has been set usable. The fifth column lists the Atomic Frequency Standard (AFS) for the specific satellite. An "Rb std", as shown in Figure 1, is defined as the Rubidium (Rb) AFS of the satellite. The voltage controlled crystal oscillator (VCXO) and the time keeping system (TKS) enable a stable and reliable performance of the satellite clock. The Mean Mission Duration (MMD) of the Rubidium Atomic Frequency Standard (RAFS) is 7.5 years ([11], pages 77-78). The "Cs std" in Figure 1 stands for the Cesium Atomic Frequency Standard (CAFS) [14].

The GPS constellation status is updated every working day. The GPS satellites are orbiting in Medium Earth Orbits (MEO) at 20,200 km altitude. The satellites are positioned in six equally spaced orbital planes, such that there are at least four satellites visible to the user at all times of the day [15]. The orbital period of the satellites is 11 hours and 58 minutes. The inclination of each orbital plane is 55° with respect to the equator ([11], pages 68-87).

The GPS satellite constellation is built on different blocks of satellites. The first one was Block I and the satellites belonging to this block were launched for initial

GPS CONSTELLATION STATUS

```
********************************************************************************
     Information in this file is retained for approximately seven
     days or until completion of the event; be aware that the
     information provided below may change.
********************************************************************************

A.  BLOCK II/IIA/IIR/IIR-M INDIVIDUAL SATELLITE STATUS

SVN  PRN
34   18  Launched 26 OCT 1993; usable 20 MAR 2018; operating on Rb std
           Set usable 20 Mar 2224 UT
             (NANU 2018015/20 MAR)
41   14  Launched 10 NOV 2000; usable 10 DEC 2000; operating on Rb std
           Scheduled unusable 18 May 0800 UT to 2000 UT for
             repositioning maintenance (NANU 2018026)
43   13  Launched 23 JUL 1997; usable 31 JAN 1998; operating on Rb std
44   28  Launched 16 JUL 2000; usable 17 AUG 2000; operating on Rb std
45   21  Launched 31 MAR 2003; usable 12 APR 2003; operating on Rb std
46   11  Launched 07 OCT 1999; usable 03 JAN 2000; operating on Rb std
47   22  Launched 21 DEC 2003; usable 12 JAN 2004; operating on Rb std
48   07  Launched 15 MAR 2008; usable 24 MAR 2008; operating on Rb std
50   05  Launched 17 AUG 2009; usable 27 AUG 2009; operating on Rb std
51   20  Launched 11 MAY 2000; usable 01 JUN 2000; operating on Rb std
52   31  Launched 25 SEP 2006; usable 12 OCT 2006; operating on Rb std
53   17  Launched 26 SEP 2005; usable 16 DEC 2005; operating on Rb std
           Scheduled unusable 12 Apr 2215 UT to 13 Apr 1015 UT for
             repositioning maintenance (NANU 2018017)
           Outage cancelled for day 102
             (NANUs 2018017, 2018019/12 APR)
55   15  Launched 17 OCT 2007; usable 31 OCT 2007; operating on Rb std
56   16  Launched 29 JAN 2003; usable 18 FEB 2003; operating on Rb std
57   29  Launched 20 DEC 2007; usable 02 JAN 2008; operating on Rb std
58   12  Launched 17 NOV 2006; usable 13 DEC 2006; operating on Rb std
59   19  Launched 20 MAR 2004; usable 05 APR 2004; operating on Rb std
60   23  Launched 23 JUN 2004; usable 09 JUL 2004; operating on Rb std
           Unusable 03 May 1423 UT to 2049 UT due to
             maintenance (NANUs 2018023, 2018025/03 MAY)
61   02  Launched 06 NOV 2004; usable 22 NOV 2004; operating on Rb std
62   25  Launched 28 MAY 2010; usable 27 AUG 2010; operating on Rb std
63   01  Launched 16 JUL 2011; usable 14 OCT 2011; operating on Rb std
64   30  Launched 21 FEB 2014; usable 30 MAY 2014; operating on Rb std
65   24  Launched 04 OCT 2012; usable 14 NOV 2012; operating on Cs std
66   27  Launched 15 MAY 2013; usable 21 JUN 2013; operating on Rb std
67   06  Launched 17 MAY 2014; usable 10 JUN 2014; operating on Rb std
68   09  Launched 02 AUG 2014; usable 17 SEP 2014; operating on Rb std
69   03  Launched 29 OCT 2014; usable 12 DEC 2014; operating on Rb std
70   32  Launched 05 FEB 2016; usable 09 MAR 2016; operating on Rb std
71   26  Launched 25 MAR 2015; usable 20 APR 2015; operating on Rb std
72   08  Launched 15 JUL 2015; usable 12 AUG 2015; operating on Cs std
73   10  Launched 31 OCT 2015; usable 09 DEC 2015; operating on Rb std
```

Figure 1: GPS Constellation Status [13].

concept validation ([11], pages 68-87). The SVNs of these satellites were from 1-11 and the mission duration was four years. The launch of these satellites started in February 1978. Three first GPS Block I satellites carried three Rb AFS with VCXO. The rest of the Block I satellites carried three Rb AFSs and one Cesium (Cs) AFS. Cesium showed a higher reliability compared to Rubidium AFS at that time [14].

The following block of satellites was Block II initial production satellites. Block IIA was upgraded production satellites ([11], pages 68-87). Block II/IIA satellites were 28 in total and were given SVNs from 13-40. Their launch started in February 1989 and the mission duration of these satellites was 7.5 years. All of the 28 satellites carried two Rb AFSs and two Cs AFSs. The Rb AFSs were equal to the ones on board the Block I satellites [14].

Block IIR were replenishment satellites for the previous blocks ([11], pages 68-87). The Block IIR satellites' launch started in 1997. These satellites carry three Rb AFSs which are modified designs of the ones on board Block I and Block II/IIA satellites.

The reliability and the mission duration of these Rb AFSs are significantly higher than the former designs because of the added temperature controller in the thermal base plate of the atomic clock. The temperature controller regulates the temperature when the temperature on board changes, to maximize the reliability [14].

Block IIR-M is a set of modernized satellites. The first satellite of the Block IIR-M was launched in September 2005 ([11], pages 68-87). These satellites have a higher output power and more downlink signals for increased robustness [14].

Block IIF are follow-on operational satellites in the GPS constellation with the first satellite launched in May 2010. These modernized satellites are expected to carry on board two Rb AFSs and one Cs AFS. The Rb AFSs on board these satellites are improved versions of the former Rb AFSs of Block IIR satellites because of an improvement in the physics package which resulted in longer life and reliability. The Cs AFSs on board these satellites are also improved designs compared to the earlier designs on board Block II/IIA satellites. The Cs AFSs have longer life time and increased short term stability because of improvements in the technology of the cesium beam tube [14].

Block III is a new generation set of GPS satellites and control segment, which was expected to be launched in 2018 [16] [17]. This program will launch advances in the development and technology of space clocks with the U.S.' program Advanced Technology Atomic Frequency Standard (ATAFS) [14].

2.1.2 Control Segment

The following section describes the control segment in more detail and explains its main functions and responsibilities. This segment monitors, controls and commands the GPS satellites. One of the main functions are to monitor the downlink navigation signals. Other important tasks are to update the navigation messages, to follow and report the satellite health and to solve possible problems with the satellites. The problems may be related to the satellite power or payload. Master Control Station (MCS), monitor stations and ground antennas are all part of the Operational Control System (OCS) and their functions are described in the following paragraphs ([11], pages 87-102).

The MCS is the mission control station of GPS satellites. The station is located at Schriever Air Force Base (AFB) in Colorado Springs, Colorado and it is operated by the U.S. Air Force Space Command, Second Space Operation Squadron (2SOPS). An alternate MCS is located in Vandenberg Air Force Base (AFB) in California for redundancy. The MCS and the alternate MCS are illustrated with a red and a yellow star in Figure 2. At the MCS the satellite health is monitored and maintained. The satellite orbits are also monitored, and in case of a vehicle failure or anomaly the MCS commands the necessary maneuvers to fix these problems. The MCS estimates the satellite clock and ephemeris parameters and generates the GPS navigation messages. The GPS time is generated and maintained by the MCS ([11], pages 87-102).

The GPS time needs to be synchronized accurately to the Coordinated Universal Time (UTC), which is maintained and monitored by the U.S. Naval Observatory (USNO). UTC time is periodically corrected with respect to the Earth's rotation. In

1972 a leap second was added to the UTC. By adding a leap second, the UTC follows more closely to the changes in the Earth's rotation. UT1 is the time corresponding to the Earth's rotation, which has had a decelerating behaviour compared to the atomic clock time. The decelerating trend of the Earth's rotation is mainly caused by tidal braking. The International Committee for Weights and Measures decided in 1956, that the difference between UT1 and UTC has to be less than 0.9 seconds. If this difference increases by 0.9 seconds, a leap second needs to be introduced to UTC [18].

January the 6^{th} 1980 at midnight UTC is epoch zero for the GPS time. At that time the GPS time was exactly equal to the UTC time [18]. The GPS Time Of Week (TOW) gives the amount of seconds that have passed in a week [19]. GPS time is equal to zero every Sunday at midnight (from Saturday to Sunday). This is the start of a new GPS week which has a total duration of 604,800 seconds ([19], [20]. The GPS week number on the week of epoch zero is equal to zero and the next week after the zeroth week is GPS week one. In other words, the GPS week is the number of weeks after the zeroth week, the week which started on January the 6^{th} 1980. Leap seconds are never adjusted to GPS time, which means that it differs compared to the periodically corrected UTC. GPS time is since December 2016 ahead of UTC by 18 seconds [18].

The monitor stations are necessary for the tracking of the GPS signal. These stations form a network covering the Earth surface operating on the L-band (1-2 GHz) frequency range. There are six Air Force monitor stations located at the places shown with a blue solid circle in Figure 2. In addition, there are 10 monitor stations from the National Geospatial-Intelligence Agency (NGA). These stations are also shown in Figure 2 with a purple solid circle. The functions of the monitor stations are to gather range and carrier measurements, navigation signals and local atmospheric data. This information is then forwarded to the MCS. The MCS then processes this data and computes the precise location of the satellites [21].

Each monitor station is equipped with a dual-frequency receiver, cesium AFSs, meteorological sensors and devices for communication. The most important functions is to gather the navigation signals from the GPS satellites, to estimate the troposphere delay with the meteorological sensors and to communicate this information to the MCS ([11], pages 90-102).

The ground antennas form a global network similar to the monitor stations. The location of the four ground antennas are illustrated in Figure 2 with the green triangles. Additionally, there are seven Air Force Satellite Control Network (AFSCN) remote tracking stations which are also pointed out in Figure 2, marked with a yellow triangle. The ground antennas are operating on the S-band (2-4 GHz) frequency range. The functions of the ground antennas are to transmit commands from the MCS to the GPS satellites, to collect telemetry data from the satellites and to forward it to the MCS. Moreover, the ground antennas perform navigation data uploads and receive payload control data ([21], [11] pages 90-102).

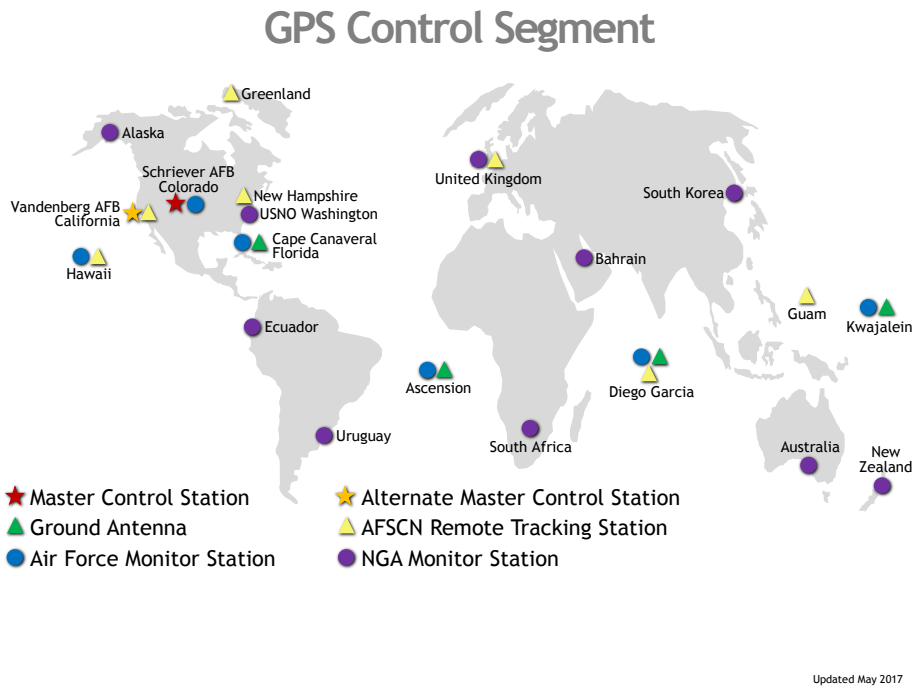

Figure 2: GPS Control Segment Map [21].

2.1.3 User Segment

The user segment is the GPS receiver which receives the GPS signals from the satellites ([11], page 103). The content of the GPS signal is described in more detail in Section 2.2. This section includes a simplified introduction to the content of the GPS signal and explains how the receiver determines its position by using the data broadcast by the GPS satellites.

The GPS satellites broadcast three pieces of information to the receiver: the Precise (P) code, the Coarse/Acquisition (C/A) code and the navigation message. The receiver computes its position and time by using the raw data, namely the P and the C/A codes which are both PRN codes. The P code is not accessible for civilian use because it is encrypted. The encrypted P code, or P(Y) code, is meant for military use only. However, the C/A code is accessible for civilian use [22].

The P code includes bits of ones and zeroes. 10.23 million bits are produced every second and the entire P code is 37 weeks long. The 37-week-long P code is divided equally into 37 parts, one week for each satellite. The P code is transferred at GPS L1 (1575.42 MHz) and L2 (1227.60 MHz) frequencies and each bit of one week P-code is repeated every seven days by each satellite. The receiver identifies which week number of the 37-week-long P-code it is receiving. This week number is equal to the SVN of the satellite, which means that the receiver can identify which satellite's signal it is reading. The P code and the C/A code are phase modulated which means that the transmission of ones and zeroes in the codes are done through changes in the carrier phase. The codes are seen as sine waves which are continuous

when there is a transition from a one chip to a one chip or from a zero chip to a zero chip. Whenever there is a change from a one chip to a zero chip the sine wave is no longer continuous and the phase shifts to the opposite direction. The C/A code is broadcast at the GPS L1 frequency transmitting 1.023 million bits every second. Each satellite transmits a unique 1023 bit C/A code every millisecond [22].

The navigation message is uploaded by the CS and it includes ephemeris information, the clock corrections, satellite health status, satellite almanac and ionospheric information. The navigation message is essential information for the receiver to be able to compute a precise position and to get information about the GPS constellation during acquisition [22]. The content of the navigation message is explained in more detail in Section 2.2.1.

The receiver needs to make a replica of the satellite's PRN code to decode it. As it was mentioned earlier, the PRN codes are phase modulated which means that the receiver needs to use phase correlation to decode the codes. The replica code's phase needs to be shifted for correlation. Maximum correlation happens when the phases of the two codes correlate. In case the phases of the codes differ by more than one chip minimum correlation occurs. The receiver needs to replicate the carrier and consider the Doppler effect. When the two dimensions code and carrier match the acquisition and tracking of the receiver are accomplished successfully. The receiver has a Right Hand Circular Polarized (RHCP) antenna to catch the GPS signal. The received signal is amplified with a low noise preamplifier to decrease noise. The GPS receiver is able to generate the code and carrier replicas of the GPS signals by using application specific hardware blocks, for example Numerically Controlled Oscillators (NCO) ([11], page 153-158). A more detailed description about the content of the GPS signal is explained in more detail in Section 2.2.

2.2 GPS Signal

GPS satellites transmit time signals at a constant rate. These signals reach an infinite amount of user receivers, because they are passively only receiving the signals. This section describes the content of the GPS signal and digs deeper into the theory given in Section 2.1.3.

The GPS signal contains codes and a navigation message which are transmitted at GPS L1 and L2 frequencies. The P(Y) encrypted military code is transmitted at both L1 and L2 frequencies and the C/A code for civilian use is transmitted only at the L1 frequency. However, new GPS civilian signals will be launched by the U.S. government: the L2C, L5 and L1C. The L2C signal is broadcast at the L2 frequency. The L2C signal was on board GPS Block IIR-M satellites in 2005, however the first broadcast of the new Civil Navigation Message (CNAV) on L2C and L5 signals started on April 28^{th} 2014 ([23], [17]). The L2C signal gives a better ionospheric correction and a more accurate position when used together with the other civilian signal C/A at L1. However, only a dual-frequency receiver can benefit from these two signals. The L2C signal is designed for commercial requirements. The L5 civilian signal is currently broadcast from 12 GPS satellites at 1176 MHz frequency. The third civilian signal makes it possible to use triple-frequency techniques to derive the

position. The same position accuracy as an augmented solution can be reached by using three signals at three different frequencies, for example by using L1 C/A, L2C and L5 together. The L5 signal is designed for Safety of Life (SoL) requirements and used in transportation applications e.g. air traffic. The L1C signal broadcast at the L1 frequency is the fourth GPS signal intended for civil use. This signal is designed for challenging environments, where the GPS signal is difficult to track and where it gets reflected easily due to different obstacles e.g. in urban environments. The L1C signal was planned to be launched with the new generation GPS III satellites in 2018 ([23], [17]).

The GPS service intended for military use is called the Precise Positioning Service (PPS). The encrypted P code, the P(Y) code, is part of the PPS and it provides high positioning accuracy for military applications [22]. The Standard Positioning Service (SPS) is the GPS service intended for civilian use. The C/A code broadcast at L1 is intended for civilian use and part of the SPS. SA was U.S. Department of Defense's action to degrade the satellite clocks for the SPS, because the civilian use code C/A provided a too accurate positioning solution with around ±20 m to ±40 m accuracy. The SA's intention was to keep the accuracy of civilian use GPS service at ±100 m in horizontal accuracy and ±175 m in vertical accuracy 95% of the time [22]. President Bill Clinton ordered the U.S. government to discontinue the SA on the 2^{nd} of May 2000. Figure 3 shows the performance of the GPS SPS before and after the decision to disrupt the SA. The plot shows the horizontal error in blue and the vertical error in red, both expressed in meters. The vertical axis is the instantaneous error and the horizontal axis gives the time of day expressed in UTC. The measurement was taken in Colorado Springs, Colorado on the day of the presidential order to cease the SA. The difference is significant after the disruption of the SA. After the disruption the Circular Error Probable (CEP) is 2.8 m and the Spherical Error Probable (SEP) is 4.6 m [9].

The GPS satellites all broadcast unique ranging codes at the same frequency. The uniqueness of these signals are possible through different modulation techniques. Binary Phase Shift Keying (BPSK) is a modulation type which is based on the multiplication between two time dependent waves: the RF carrier and the data waveform. The product of these two factors is the BPSK-signal, the modulated RF carrier, shown in Figure 4. The RF carrier's phase is either shifted by 180° or continues vibrating unmodulated depending on the value of the data waveform which changes between +1 and -1. T_b in Figure 4 is the bit period of the data waveform given as

$$T_b = 1/R_b, \tag{1}$$

where R_b is the data rate expressed in bits per second ([11], pages 113-114).

Another modulation type is called the Direct Sequence Spread Spectrum (DSSS), illustrated in Figure 5. DSSS is similar to the BPSK modulation type explained above because the unmodulated RF carrier and the data waveform are also part of the modulation sequence. However, a new waveform has been added in the sequence

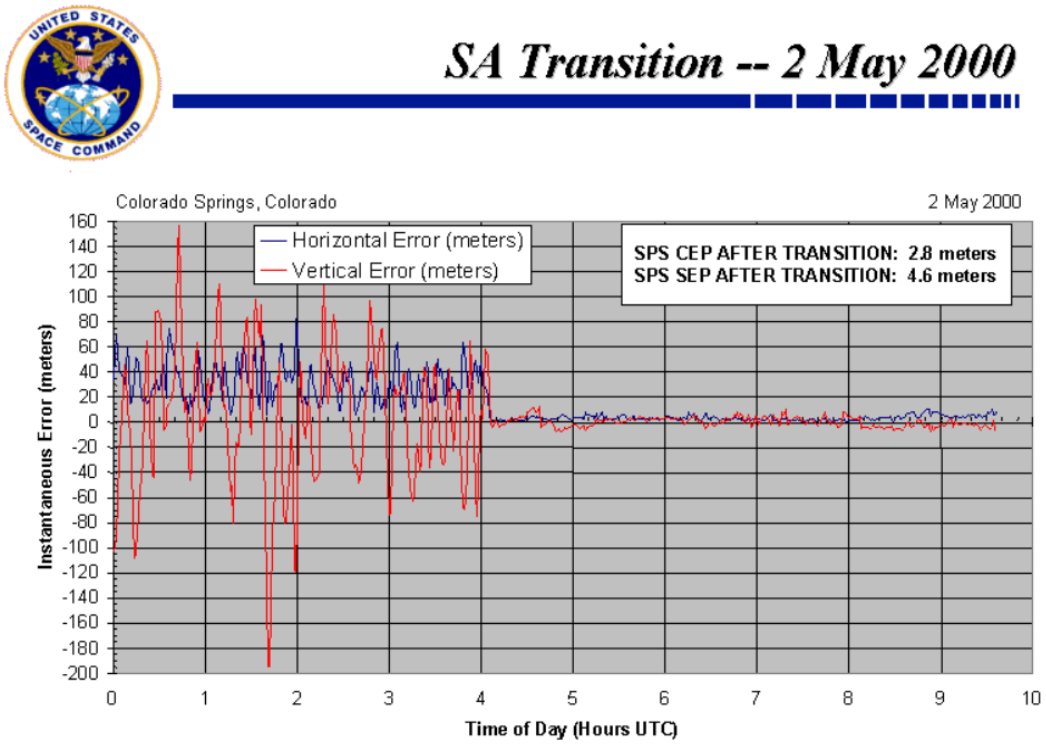

Figure 3: GPS SPS performance on May 2^{nd} 2000 before and after the disruption of SA. The blue curve shows the horizontal error in meters and the red curve shows the vertical error in meters as functions of the time of day in UTC time [9].

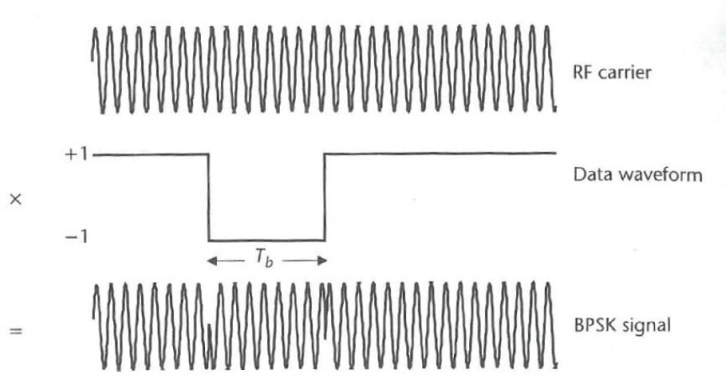

Figure 4: BPSK Modulation ([11], page 114).

called the spreading waveform, shown in Figure 5. The spreading waveform looks similar to the data waveform because its value changes also between +1 and -1. The difference between these two is the much higher bit rate of the spreading waveform compared to the data waveform. The shortest time between two bits is called the chip period, T_c, which is shown in Figure 5. The spreading waveform is also called the PRN waveform or the PRN code. The DSSS modulation type is used mainly in satellite navigation because multiple PRN codes can be transmitted at the same

frequency simultaneously, and the receiver is able to distinguish them because of the different spreading waveforms of each satellite. This is called Code Division Multiple Access (CDMA) ([11], pages 114-115).

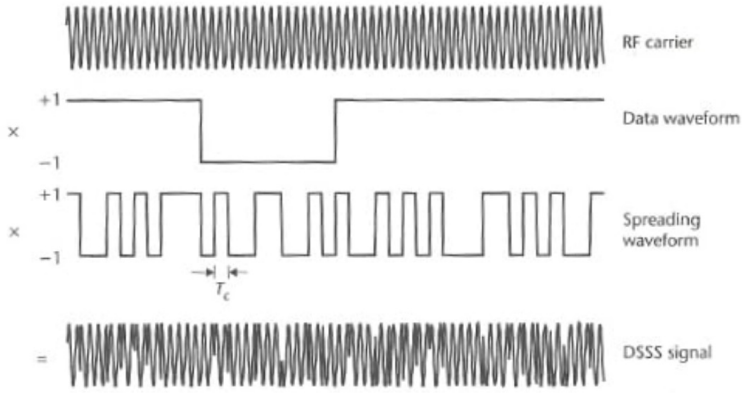

Figure 5: DSSS Modulation ([11], page 114).

2.2.1 Navigation Message

The P(Y) and C/A codes described in the earlier sections tell the receiver the time when the signal was sent from the satellite, in other words the transmission time, and the location of the satellite at that time. These codes are modulated and the data flow rate is 50 bits per second. The navigation message is a necessary part of the GPS signal for the receiver to compute a precise position ([11], pages 142-145). Its content is described more thoroughly in this section.

Figure 6 illustrates the content of the navigation message, which is broadcast at a 50 Hz frequency rate containing 37,500 bits of data with 25 frames in total. All frames contain 5 subframes with 1500 bits of data each. The subframes include 10 words with 300 bits of data each and a word contains 30 bits of data. Subframes 1 to 3 have one page of data repeated on all 25 frames, whereas subframes 4 and 5 have 25 different subframes of data on each page ([11] pages 142-145, [22]).

The first word of each subframe is denoted TLM, which stands for telemetry. This word always starts with the 8-bit sequence 10001011. Each telemetry word starts with this sequence, which helps the receiver to know the start of each subframe. Additionally, the TLM provides the receiver with information about how old the ephemeris data is. The second word of each subframe is called HOW, which stands for handover word. This word contains the GPS TOW of the transmission time and the position of the satellite at this time. The HOW also tells the receiver which subframe number it is reading [22].

Words 3 through 10 in subframe 1 contain information about the clock correction, the GPS week and the satellite health status. The clock correction is uploaded by the control segment. It gives the difference between the satellite clock and the ground station's atomic clock. The cesium and rubidium oscillator clocks on

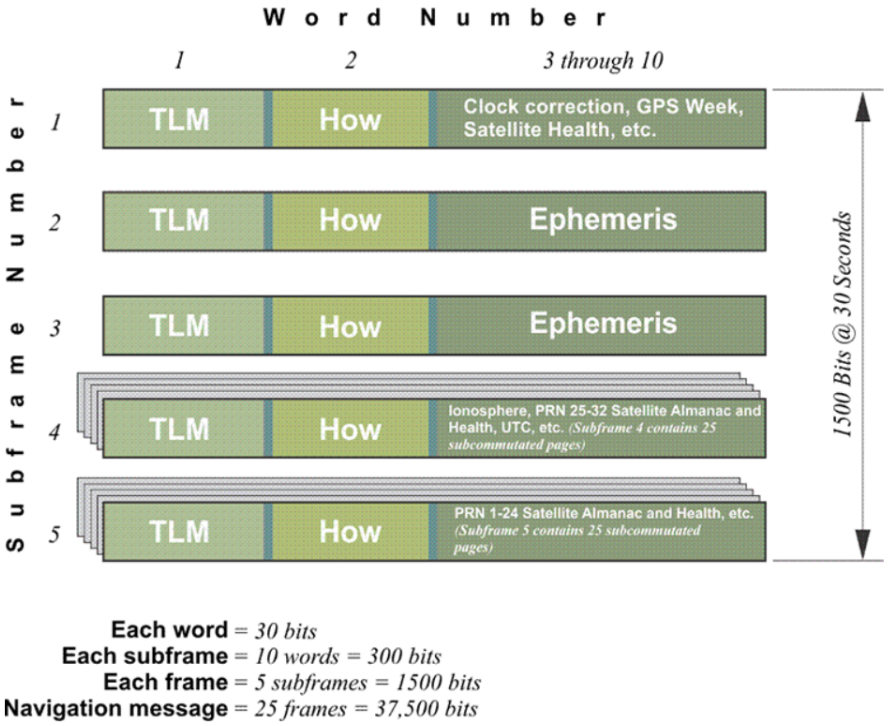

Figure 6: The Navigation Message [22].

board the satellites have a tendency to drift compared to the atomic clocks at the ground stations. The control segment needs to verify that the difference between the satellite clock time and the ground station time is not more than 1 microsecond. This might seem small however a clock error, ΔT_{error}, of 1 microsecond in a signal travelling at the speed of light causes a range error, ΔR_{error}, of approximately 300 m, $\Delta R_{error} = c \times \Delta T_{error} = 2.99792458 \cdot 10^8 m/s \times 1.0 \cdot 10^{-6} s \approx 300m$, where c stands for the speed of light ([22], [24]). The control segment uploads the offsets to the satellites which then transmit them further to the receiver as part of the navigation message. Satellite clocks are affected by their environment in orbit e.g. changes in gravity and fluctuations in the on board temperature of the satellite. These factors may cause the clock drift on board the satellites to increase [22].

Subframes 2 and 3 both contain ephemeris in words 3 through 10. Ephemeris data provides the parameters required for the receiver to determine the precise position of the satellite relative to the Earth when it transmitted the GPS signal. The ephemeris provides the Keplerian elements: the Right Ascension, RA, the semimajor axis, a, the eccentricity, e, the right ascension of ascending node, Ω , the argument of perigee, ω, the true anomaly, T, of the satellite at the transmission time. The receiver computes the satellite's location in Earth-Centered, Earth-Fixed (ECEF), World Geodetic System 1984 (WGS84) coordinate frame. It is good to remember that the satellite orbit is never a perfect elliptical shape and may change its shape due to e.g. gravity and solar wind [22].

Subframe 4 contains in words 3 through 10 data about the ionosphere, the satellite

almanac and health of PRN 25-32 and the UTC. Atmospheric information, such as ionospheric details, are necessary for the receiver to be able to correct for the signal attenuation due to the ionosphere. The satellite almanac tells the receiver where the satellites are located. The control segment uploads this information daily to the satellites. It is useful for the receiver to have the satellite almanac because it takes a much shorter time to read them compared to the ephemerides. It takes 12.5 minutes for the receiver to acquire the entire navigation message with 37,500 bits at a frequency of 50 Hz. The almanac contains coarse orbital elements for each satellite for the receiver to be able to compute close enough estimates of the satellite positions. By using the satellite almanac the receiver is able to make a faster position fix than waiting for 12.5 minutes to obtain the entire navigation message. The satellite health describes the operational status of the satellite. This information is necessary for the receiver to be able to evaluate if the data from the satellite is reliable or if it should be discarded. Subframe 5 contains in words 3 through 10 satellite almanac and health of PRN 1-24 as well as almanac reference time and week number ([22], [11] pages 142-145).

2.3 Receiver Position

This section covers the fundamental relations required by the receiver to be able to solve its position in space and time. The receiver needs to compute four unknown parameters: x_u, y_u, z_u coordinates and the time offset t_u, where u stands for the vector denoting the receiver's position with respect to the center of the Earth. The vector u is expressed in the ECEF coordinate system. The receiver needs four different GPS signals to be able to get four different equations to solve the four unknowns ([11], pages 50-58).

The satellite atomic clocks have an offset compared to the system time, the precisely controlled time of the ground stations. Therefore, there is an offset between the satellite atomic clocks and the system time, which is denoted by δt. This offset needs to be considered when computing the receiver position. Another time offset is the difference between the receiver time and the system time, which is denoted t_u. The distance between the satellite and the receiver is called Pseudorange (PR), where pseudo stands for false or untrue. It is a false range because it gives the false distance between the satellite and the receiver due to the time offsets of the nonsynchronized clocks. The system time at which the signal is transmitted from the satellite is given the symbol T_s. T_u stands for the system time when the signal was received by the receiver. The geometric range, the true range between the satellite and the receiver is equal to

$$r = \mathrm{c}(T_u - T_s) = \mathrm{c}\Delta t, \tag{2}$$

where c stands for the speed of light ($\approx 3 \times 10^8$ [m/s]). Equation 2 gives the true range with respect to the system time. The PR includes the time offsets of the satellite clock and the receiver clock and gives the approximate range between the satellite and the receiver. It is equal to

$$\rho = \mathrm{c}[(T_u + t_u) - (T_s + \delta t)] = \mathrm{c}(T_u - T_s) + \mathrm{c}(t_u - \delta t) = r + \mathrm{c}(t_u - \delta t). \quad (3)$$

As mentioned in earlier sections, the task of the control segment is to provide the user receiver with time corrections of the received signal in the navigation message. This time correction provides the δt time offset required to get the signal transmission time in system time. This means that the δt is negligible in Equation 3 because when the receiver decodes the navigation message it corrects for this time offset ([11], pages 50-58). The PR equation, Equation 3, simplifies then to

$$\rho = r + \mathrm{c}t_u. \quad (4)$$

The true range, r, is composed of the satellite's and the receiver's position in three dimensional space. The PR from the j^{th} satellite is then expressed by

$$\rho_j = \sqrt{(x_j - x_u)^2 + (y_j - y_u)^2 + (z_j - z_u)^2} + \mathrm{c}t_u. \quad (5)$$

At least four equations are required of this form, Equation 5, for the receiver to compute its position. These four equations are solved by either using closed-form solutions, linearization methods through iteration or by applying Kalman filtering ([11], pages 50-58).

The closed-form solution is based on a method of solving two linear equations. One linear equation containing a range difference and another linear equation containing the PR [25]. The linearization method uses a Taylor series approximation of the position offset which is caused by the time offset of the receiver compared to the system time ([11], page 55). The Kalman filtering method makes a statistical estimate of the position by using two consecutive measurements ([11], pages 466-467).

2.4 GPS Errors

Different methods are used to decrease the GPS errors to get a more accurate position, namely by using DGPS and SBAS. Before describing these techniques in more detail the GPS errors are identified and explained.

All satellite clocks have an offset compared to the system time, which is maintained by the control segment. The navigation message contains this information necessary for the receiver to compensate for this offset. The range error due to the satellite clock offset is in the range of 0.3-4 m. The error increases with the age of the satellite and its payload. Relativity plays also a role in the offset between satellite clocks and the clocks on the ground. The relativistic effects increase when the satellite velocity and the gravitational potential deviate. The satellite velocity is not constant when it travels in its orbit. At perigee, the satellite velocity is higher than when it is at apogee because here it gets closer to the Earth's gravitational field where it loses gravitational potential. The consequence of these factors is that the satellite clock at perigee runs more slowly. At apogee, the satellite loses kinetic energy while gaining gravitational potential because it moves further away from the Earth's gravitational

field. The satellite clock runs faster at apogee due to these factors. ([11], pages 304-308, 381-382).

The orbital parameters uploaded from the ephemerides of all satellites give an approximate location of the satellite at the transmission time. This location deviates from the true position of the satellite by around 1-6 m. The ephemeris error induces a measurement error in both the PR and carrier phase measurements. The ground stations monitor the satellite position easily in the radial direction, in the direction from the satellite to the center of the Earth. However, in the along-track and the cross-track directions the ground stations are not able to identify the position errors so easily. The along-track direction is in the direction of motion of the satellite orbiting the Earth and the cross-track direction is perpendicular to the radial and the along-track vectors. This offset between the approximate orbital location of the satellite and the true position of the satellite give an ephemeris error of around 0.8 m (1σ). The ephemeris errors change depending on the position of the receiver. Another receiver obtaining the same satellite signal at a different location will not obtain the same ephemeris data compared to another receiver. However, a ground station located in the proximity of the receiver is able to correct for the ephemeris errors because the data does not deviate much nearby ([11], pages 305-306, 382-384).

The atmosphere delays the electromagnetic wave propagation. The speed of the signal is slowed down and obstructed from its path because of different particles in the atmosphere. The ionosphere starts from 70 km altitude and reaches an altitude of 1,000 km above the Earth's surface. Free electrons are present in the ionosphere because of the ionizing effect of the sun rays. The more free electrons are present in the ionosphere, the larger is the ionospheric delay on the GPS signal. The amount of free electrons in the ionosphere depends on e.g. solar activity, the location of the receiver, the time of day, the satellite elevation angle, the magnetic activity and the season. The ionosphere is a source of error on the PR and the carrier phase measurements with a magnitude of around 7 m (1σ). A dual-frequency receiver is able to eliminate the ionospheric delay effectively by measuring the range at two different frequencies. The ionospheric delay is related to the frequency as expressed in Equation 6. Two range measurements at two different frequencies provide an ionospheric-free PR solution as

$$\rho_{ionospheric-free} = \frac{\rho_{L2} - \gamma\rho_{L1}}{1-\gamma}, \tag{6}$$

where $\gamma = (f_{L1}/f_{L2})^2$. f_{L1} is the L1 frequency and f_{L2} is the L2 frequency. ρ_{L1} is the PR measurement at L1 and ρ_{L2} is the PR measurement at L2 ([11], pages 310-314).

When the electromagnetic wave penetrates the troposphere, its path is obstructed depending on the conditions of the tropospheric layer. The troposphere is the layer of the atmosphere closest to the Earth's surface and below 70 km altitude. The delay caused by the troposphere varies depending on the temperature, pressure and relative humidity. These conditions may slow down and change the path of the electromagnetic wave. The tropospheric error varies between 2.4 m and 25 m depending on the elevation angle of the satellite. The tropospheric refractivity

consists of two components: the dry component and the wet component. The dry component of the tropospheric refractivity is caused by the dry air in the troposphere. It covers 40 km of altitude and 90% of the tropospheric error. The wet component is composed of the water vapour in the troposphere and it covers 10 km of altitude. This component is less predictable than the dry component. The tropospheric error is corrected by using the measurements from a ground station located in the proximity of the receiver. The tropospheric delay is approximately the same for the ground station and the receiver when they are located in the proximity of each other. Other methods for correcting this error is by applying different mapping functions to model the dry and wet components of the troposphere ([11], pages 314-319).

Receiver noise is also a source of error in the PR and the carrier phase measurements. This noise is caused mainly by the receiver tracking loops: the Phase Lock Loop (PLL) and the Delay Lock Loop (DLL). The PLL is the tracking loop that keeps the carrier phase error zero between the replica and the satellite signal. The main sources of error in a phase tracking loop are phase jitter, thermal noise and dynamic stress error. The DLL is the tracking loop which tracks the code and minimizes the error between the code replica and the satellite signal. The error sources for a code tracking loop are thermal noise range error jitter and dynamic stress error. The code tracking loop induces an error around 1 dm (1σ) and the phase tracking loop causes an error of around 1.2 mm (1σ) ([11], pages 155-179, 183-200, 319).

Multipath occurs when the GPS signal gets reflected from a surface before reaching the receiver. This is common in urban environments. When the GPS signal is obstructed on its way to the receiver, its path becomes longer and delayed. Shadowing happens when the GPS signal penetrates a surface or obstacle before reaching the receiver. In some cases, a signal may experience both multipath and shadowing e.g. after reflecting from a building's wall, the signal travels through a window or a tree, before reaching the user. Although the path of a shadowed signal may be shorter than that of a multipath signal, the multipath signal may have a higher power than the shadowed signal. The magnitude of the error induced on the carrier phase and PR measurements depends on the power of the multipath signal and on its delay. A low powered multipath signal causes a smaller measurement error than a high powered multipath signal. It is challenging to estimate the magnitude of a typical multipath error, however a common approximation for the PR error is around 20 cm (1σ) and the carrier phase error is around 2 cm (1σ) ([11], pages 279-292, 319).

3 Augmentation Techniques

Safer maritime navigation techniques for solving the challenges in the sea level are presented in this chapter. In Finland, vessels use the DGPS service provided by LiVi. This augmentation system is capable of augmenting the GPS signal to obtain robust PNT solutions. SBAS is another augmentation method that also provides robust PNT solutions. The SBAS used in Europe is called EGNOS. This chapter gives more information about these techniques and the use of the systems in Europe. The characteristics and the decoding of the augmentation messages from LiVi and EGNOS are described in this chapter.

3.1 Differential GPS (DGPS)

The previous chapter described the different errors involved with the receiver measurements. This section presents a technique to mitigate these errors. The technique is DGPS which relies on the similarity of GPS errors between receivers located close by each other. The user may upload corrections from one or multiple DGPS Reference Stations (RSs).

These RSs are equipped with GPS receivers which continuously measure raw PR and carrier phase of visible satellites. Some GPS errors are easily corrected for at the DGPS stations because their locations are known and meteorological data is accessible. The DGPS stations measure their location with their receivers and are able to know the magnitude of the measurement error because of the accurately known location of the station. The difference between the measurements and the accurate location of the station gives the measurement error at a specific time. This information is then broadcast to a user located close by, through a radio link between 300 kHz and 2000 MHz, or through the Internet ([11], pages 379-383).

Corrections are provided for PR, carrier phase, satellite clock and ephemeris of the user measurements. The user may also replace its satellite clock and ephemeris data with the ones observed at the DGPS stations. In addition, these stations provide the user with the accuracy of each correction and with the health status of the station providing the corrections. In this way, the user knows whether the corrections are valid or not. Similarly, the health status of each visible satellite is broadcast to the user. The location of the DGPS station is also broadcast together with the meteorological data of the station. These corrections are only available for post-processing because there is always a delay in the radio link between the DGPS stations and the user ([11], pages 379-383).

The characteristics of the corrections are categorized in different types of DGPS techniques. Absolute differential positioning is a technique which provides the DGPS corrections in the ECEF coordinate system. This coordinate system is defined as a coordinate frame which rotates with the Earth. The Earth's equatorial plane is the xy-plane of this coordinate system. The positive x-axis is aligned in the direction of 0° longitude and the positive y-axis is aligned in the direction of 90° latitude in the East direction. The z-axis points in the direction of the North Pole and it is perpendicular to the equatorial plane. These corrections are easily applied by the

user because the user receiver computes its position in the same coordinate system. Aircraft and maritime applications use this technique in challenging environments ([11], pages 28, 379-383).

Relative differential positioning is a DGPS technique which provides the corrections with respect to the DGPS station. The location of the station in the ECEF coordinate frame is not known as accurately as in absolute differential positioning. This technique may be used for example if the locations of two vehicles are known with respect to each other. Corrections provided to a single user's measurements through relative differential positioning is not so useful because the RS's location in the ECEF coordinate frame may deviate ([11], pages 379-383).

It was mentioned earlier in this section that the GPS errors are mitigated by applying corrections from DGPS stations located in the proximity of the user. However, the definition of proximity when applying DGPS corrections is still unclear. The simplest type of DGPS technique is applied when the distance, or baseline, between the user and the DGPS station is around 10-100 km. This technique provides corrections to a user from one or multiple RSs. When the baseline gets larger than 100 km and up to 1000 km the DGPS technique applied is called regional area differential positioning. This technique combines corrections from multiple DGPS stations and applies different algorithms to provide correction data to users within this range. For a baseline larger than 1000 km, the DGPS corrections are broadcast with wide area differential positioning ([11], pages 379-383).

A DGPS station providing code-based corrections is called a code-based DGPS system. The user uploads corrections for its code-based PR measurements. This technique provides the user with a positioning accuracy of a few decimeters. A more accurate position is assured by using carrier-based differential positioning. It provides an accuracy of a few millimeters ([11], pages 379-383).

3.1.1 LiVi DGPS Service

The GPS signal alone is not enough to navigate safely during critical maritime operations. The signals received from GPS alone provide no up-to-date integrity information. Accuracy and integrity are important factors especially in merchant shipping. A DGPS service provides up-to-date corrections and integrity information for the GPS signals. The DGPS RSs of LiVi provide correction data for maritime navigation in the Finnish watercourse. The corrections are given according to international standards. The correction data is broadcast at a 300 kHz frequency and the messages follow the International Telecommunication Union's (ITU) recommendation ITU-R M.823-3 [26].

The DGPS service provided by LiVi is meant for maritime services and it is available for free. Radio beacons are used to broadcast the corrections. The specifications of the DGPS service stations in Finland are shown in Figure 7. The bit rate is 100 bps and each message includes integrity information. Corrections are provided for no more than nine satellites at a time. The elevation angle of these satellites needs to be greater than 7°. A warning message is sent if the error is greater than 10 m for more than 20 s. The recipient will receive the warning message within 10 s. The

accuracy of the DGPS service depends on the quality of the user receiver [27]. The LiVi DGPS service ensures an accuracy of less than 10 m 95% of the time. However, in practice the accuracy is close to 1-2 m 95% of the time [26].

Figure 7 lists information about all nine RSs, namely their location in latitude and longitude, their coverage area, the transmitting station ID, the broadcast frequency and the bit rate [26]. The coverage area is a rough estimate of how radio waves propagate over open sea. When radio waves travel over land the coverage area decreases significantly [27]. The Vessel Traffic Service (VTS) centre is responsible of the safety at sea and of the prevention of accidents and environmental damages. There are three VTS control centers in Finland: in Turku, in Helsinki and in Lappeenranta. The VTS centre surveys the DGPS service provided by LiVi. If the VTS notices a malfunction in the DGPS service it gives a sea warning ([27], [28]). Section 3.1.2 describes in detail the standards of the DGPS correction messages and the decoding of these messages.

Transmitting Station	ID	Reference Station ID	Location (Lat / Lon)	Coverage area (km)	Frequency (kHz)	Bit rate (bit/s)
Porkkala	400	600	59°58'N / 24°23'E	250	293.5	100
Mäntyluoto	401	601	61°36'N / 21°28'E	250	287.5	100
Puumala	402	602	61°24'N / 28°14'E	70	290.0	100
Outokumpu	403	603	62°41'N / 29°01'E	70	304.5	100
Turku	404	604	60°26'N / 22°13'E	200	301.5	100
Marjaniemi	405	605	65°02'N / 24°34'E	250	314.5	100
Klamila	406	606	60°30'N / 27°26'E	250	287.0	100
Haarajoki	407	607	60°31'N / 25°10'E	250	292.5	100
Kokkola	408	608	63°52'N / 23°11'E	250	290.5	100

Figure 7: DGPS Stations in Finland [26].

3.1.2 Radio Technical Commission for Maritime Services (RTCM)

The Radio Technical Commission for Maritime Services (RTCM) is an international non-profit organization for the scientific, professional and educational communities with members worldwide. In 1947 it was an advisory committee of the U.S. government however now it is acting as an independent organization [29].

LiVi offers correction data in the form of different RTCM messages sent from the RSs listed in Figure 7. The RS uses a Minimum Shift Keying (MSK) modulator and a reference receiver to produce the correction messages. The MSK modulation gives a linear 90 degree phase delay for a binary 0 and a linear 90 degree phase advance in case of a binary 1. This is a digital modulation based on Continuous Phase Frequency Shift Keying (CPFSK). The corrections are given as C/A code Pseudorange Corrections (PRCs) for each visible GPS satellite. The Integrity Monitor (IM) is responsible for verifying the correction messages being broadcast by the RS. IM broadcasts position and PRC alarms when the data is not within a certain tolerance. The Control Station (CS) orders actions to correct for anomalies in the corrections and the service. CS collects and stores the data broadcast by RS and IM for further processing. The Reference Station/Integrity Monitor (RSIM) messages are transmitted through the RSIM Interface Module (RIM) which is able to provide control and monitoring actions. The analysis of this thesis focuses on the PRC data processed and displayed by the RS in RSIM message number 13. The IM broadcasts, in RSIM message number 19, the integrity information of the correction data ([30], pages 1-49).

Figure 8 shows the message composition of the RSIM message number 13. This message provides the RS correction data. The message is a composite message in groups of three PRNs. This means that for each line of message there is up to three different corrections for three PRNs. Each 13^{th} RSIM message starts with the denotation $PRCM. This is followed by the message number, in this case the number 13. In the first field, denoted by 1 in Figure 8, the total number of messages is given. The second field gives the message number (message #) and the third field provides the UTC time, which is given in the form hhmmss.ss, where hh denotes the hours, mm stands for the minutes, ss indicates the seconds and .ss gives the hundredths of a second (centiseconds). Field number 4 gives the PRN number of the correction data. The PRC in field number 5 is the PRC for the PRN in field 4. The PRC is expressed in meters. The minimum requirements that the PR measurements and corrections need to meet are a L1 C/A Code signal power level of at least -160 dBW, an elevation angle larger than 7.5 degrees, a minimum tracking time of 120 seconds, a minimum of four visible satellites and a maximum of 12 visible satellites. Field 6 shows the Range Rate Correction (RRC) of the PRN in meters per seconds and field 7 provides the PR Acceleration in meters per seconds squared. The User Differential Range Error (UDRE) is displayed in field number 8, expressed in meters. UDRE is an estimate of the 1σ error of the differential PRC. This value depends on e.g. the carrier to noise ratio (C/N_0) of the GPS signal. RTCM Modified Z-Count is in field number 9 and the Issue of Data (IOD) in field a. RTCM Modified Z-Count is the time of the DGPS correction message expressed in GPS time ([30], pages 19-63).

RSIM #13: REFERENCE STATION CORRECTION DATA

USAGE: RS uses to report most recent DGPS computations at time message is originated.

```
FIELD #  1 2 3         4 5   6   7  8    9   a b c   d   e   f   g   h i j
         ^ ^ ^         ^ ^   ^   ^  ^    ^   ^ ^ ^   ^   ^   ^   ^   ^ ^ ^
$PRCM,13,x,x,hhmmss.ss,x,x.x,x.x,x.x,x.x,x.x,x.x,x,x,x.x,x.x,x.x,x.x,x.x,x.x,x,x,x.x,

k   l   m   n   o
^   ^   ^   ^   ^
x.x,x.x,x.x,x.x,x*hh<CR><LF>
```

WHERE:

1 - Total Number of Messages
2 - Message #
3 - UTC Time of Message
4 - PRN #
5 - PRC
6 - RRC
7 - PR Acceleration
8 - UDRE
9 - RTCM Modified Z-Count
a - IOD
b - PRN #
c - PRC
d - RRC
e - PR Acceleration
f - UDRE
g - RTCM Modified Z-Count
h - IOD
i - PRN #
j - PRC
k - RRC
l - PR Acceleration
m -UDRE
n - RTCM Modified Z-Count
o - IOD

NOTE: Composite message, in groups of 3 PRN's.

Figure 8: RSIM#13: RS Correction Data message decoding according to RTCM 10401.2 ([30], page 63).

The IOD is the identification of the set of data received from a satellite. The IOD is unique for each satellite and it enables the receiver to identify which satellite's data it is decoding. On each page of the ephemeris, the clock correction and the almanac, and the IOD are given to facilitate the identification process of the receiver [31]. The same information from fields 4 through a is repeated over the following fields from b through o for the two other PRNs for which corrections are received for ([30], page 63).

Figure 9 represents the 19^{th} RSIM message broadcast by the IM. This message includes PRC integrity information. The 19^{th} RSIM message is a composite message of three different PRNs similar to RSIM #13. The message line starts with the denotation $PRCM followed by the message number, in this case by the number 19. The first field provides the total number of messages and field 2 gives the message number. The UTC time is expressed in field 3 in the hhmmss.ss format. The PRN number is in field 4 and the PR and the Range Rate (RR) residuals in fields 5 and 6 respectively. The PRC given in RSIM #13 includes an error which the IM needs to monitor. It compares the correction data with the true ranges computed by the known IM position. The error between the correction data and the true range computed at the IM is the PR residual value displayed in field 5. This value is expressed in meters. The RR residual is presented in meters per second and it is defined as the difference between the RR computed at the IM's known position and the RRC data provided in RSIM #13. When the PR residual exceeds 30 cm in an open sky environment, an alarm is triggered. In an urban environment the PR residual alarm is triggered when the PR residual increases 80 cm. Field 7 issues the Correction Quality Indicator (CQI) and it is computed according to

$$\mathrm{CQI}(t_2) = |\mathrm{PRC}_{t2} - [\mathrm{PRC}_{t1} + \mathrm{RRC}_{t1} * (t_2 - t_1)]|, \tag{7}$$

where t_1 is synchronized with the GPS time of the correction message given in RSIM #13 in field 9 and named Modified Z-Count. t_2 is the GPS time for the following PRC of the same satellite as at time t_1. Similarly, PRC_{t1} and PRC_{t2} denote the PRC at times t_1 and t_2 respectively and RRC_{t1} is the RRC at time t_1. The CQI is typically less than 1.4 m (1σ) in maritime navigation and less than 0.6 m (1σ) in Multi-Use Services. These values are valid when the data rate is 100 bps and at least nine satellites are corrected. Field 8 displays the PR variance estimate and the correction age is issued in field 9. The correction age is defined as the difference between the correction data GPS time, denoted by modified Z-Count in RSIM #13, and the GPS time at the IM. The same information provided in fields 4 through 9 is given for the following two PRNs in fields a through l. The residuals in this message are from SVs that are above the elevation mask angle. In case the residuals in RSIM #19 are zero, the PRN is prevented by the IM ([30], page 20-112).

RSIM #19: INTEGRITY MONITOR CORRECTION DATA

USAGE: IM sends to provide instantaneous values of detailed DGPS data to the CS.

```
FIELD #   1 2 3          4 5    6    7    8    9    a b
          ^ ^ ^          ^ ^    ^    ^    ^    ^    ^ ^
$PRCM,19,x,x,hhmmss.ss,x,x.x,x.x,x.x,x.x,x.x,x.x,x,x.x,

c    d    e    f    g h    i    j    k    l
^    ^    ^    ^    ^ ^    ^    ^    ^    ^
x.x,x.x,x.x,x.x,x,x.x,x.x,x.x,x.x,x.x*hh<CR><LF>
```

WHERE:

1 - Total Number of Messages
2 - Message #
3 - UTC Time
4 - PRN #
5 - PR Residual
6 - RR Residual
7 - Correction Quality Indicator
8 - PR Variance Estimate
9 - Correction Age
a - PRN #
b - PR Residual
c - RR Residual
d - Correction Quality Indicator
e - Variance Estimate
f - Correction Age
g - PRN #
h - PR Residual
i - RR Residual
j - Correction Quality Indicator
k - Variance Estimate
l - Correction Age

NOTES:
1) Composite message, in groups of 3 PRN's.
2) Correction age is the difference between the modified Z-Count of correction and the GPS time at the IM when correction is applied.
3) Setting this message's output interval to "0" with RSIM #1 will cause it to be generated each time a new RTCM #1 or #9 is received.
4) If the RS has generated a correction for a satellite temporarily blocked at the IM, residuals will be left as null fields.
5) Only SV's above the Elevation Mask Angle are included.

Figure 9: RSIM#19: IM Correction Data according to RTCM 10401.2 ([30], page 69).

3.2 Satellite-Based Augmentation System (SBAS)

The earlier sections covered the DGPS and described how this system mitigates GPS errors. Another augmentation technique to mitigate GPS errors is SBAS. This section describes the architecture of SBAS and how this system provides the corrections to the user. This section also includes a description of EGNOS.

Similarly to DGPS, SBAS consists of a network of RSs covering a wide area. These RSs gather data from visible GPS satellites and broadcast the information further to master stations. Integrity and differential corrections for each visible GPS satellite are computed by the master stations. After computing this information the master stations send this information further to ground stations, which then broadcast this information further to the GEO satellites together with the navigation message. These satellites broadcast correction data for GPS satellites and to users within the coverage area ([11], pages 355-359).

SBAS is used and implemented worldwide. They are operational in the U.S., Europe, Japan and India. SBAS in the U.S. is called the Wide Area Augmentation System (WAAS). In Europe SBAS is provided by EGNOS. The Japanese SBAS is called Multi-functional Satellite Augmentation System (MSAS) and the Indian SBAS is called GPS and GEO Augmented Navigation (GAGAN). SBAS systems under development are Russia's System for Differential Corrections and Monitoring (SDCM), the Chinese Satellite Navigation Augmentation System (SNAS) and the South Korean Wide Area Differential Global Positioning System (WADGPS) [32].

The European Space Agency (ESA) initiated the agreements of a European SBAS in 1995. After agreements between ESA, the European Commission (EC), Eurocontrol and national Air Navigation Service Providers, the development of EGNOS started in 1999. EGNOS was handed over to the EC on the first of April 2009 and the correction data was broadcast freely for the first time to the public on the first of October 2009 [33].

EGNOS is composed of a ground segment, a support segment, a space segment and a user segment. The ground segment contains 40 Ranging Integrity Monitoring Stations (RIMS), two Mission Control Centres (MCC) and six Navigation Land Earth Stations (NLES). The EGNOS Wide Area Network (EWAN) is the communication link between these three components of the ground segment. The RIMS stations are located all over Europe and they gather data from GPS satellites. The gathered data is then sent to the MCC through the Central Processing Facilities (CPF) every second. At the MCC the data is processed and the corrections are generated in the form of EGNOS messages. These messages are then forwarded to the NLES by the CPF of the MCC. The NLES uplink these EGNOS messages to the GEO satellites. The support segment consists of a Performance Assessment and Checkout Facility (PACF) and the Application Specific Qualification Facility (ASQF). The support segment is controlled by the EGNOS Service Provider: the European Satellite Service Provider (ESSP). PACF is together with the EGNOS management responsible for the performance and the assessment of the EGNOS service. It provides troubleshooting and commands necessary actions to maintain service. ASQF is the part of the support segment necessary for the civil aviation and aeronautical certification authorities.

These parties require qualification, validation and certification of EGNOS. Three GEO satellites are part of the space segment of EGNOS. These satellites downlink EGNOS messages to the user segment at the L1 (1575.42 MHz) frequency band [34]. These satellites are in 36,000 km altitude circular orbits. There are two Inmarsat-3 satellites and one Artemis satellite by ESA [33]. Inmarsat is an initiative established by the IMO in 1979 for safer maritime navigation [35]. The user segment includes anyone with an EGNOS enabled receiver. There are many applications that benefit from EGNOS services in e.g. maritime, agriculture and aviation applications [34].

EGNOS provides three services namely the Open Service (OS), the Commercial Data Distribution Service (CDDS) and the SoL service. The OS provides EGNOS data freely to anyone in Europe with an EGNOS enabled GPS receiver. The OS ensures a horizontal position accuracy of 1 to 3 m and a vertical position accuracy of 2 to 4 m for GPS [33].

The CDDS is a service meant for professional users and provides EGNOS data through EDAS. The restricted service provides the user with raw GPS, GLONASS and EGNOS observation data with a one second update rate. Navigation messages are provided from the RIMS stations and the NLES stations. In addition, the user may upload EGNOS augmentation messages from EDAS which are broadcast from the EGNOS GEO satellites [36]. This service gives the user integrity data, GPS clock data, ephemeris and ionospheric corrections [33]. The EGNOS data in EDAS is provided in either Service Level 0 (SL0) or in Service Level 2 (SL2) depending on the data format. The data is encoded in Abstract Syntax Notation number One (ASN.1) format for SL0 and in RTCM 3.1 standard in SL2 [36]. ASN.1 is a format used to transmit data independent of the language, physical representation and the application. This format is used to encode abstract data types [37]. RTCM 3.1 is the RTCM standard version 3.1 specified by the RTCM [29]. There are multiple services of EDAS depending on the application of the user. The EDAS Data Filtering Service provides SL0 and SL2 data from certain RIMS at 1 Hz or 1/30 Hz. The EDAS Signal in Space through the Internet (SISNet) service gives the user EGNOS messages through the Internet. This data is provided according to the SISNeT protocol and the user needs to be registered to access the service. EGNOS messages are also available for post-processing purposes through the EDAS FTP. This service provides EDAS/EGNOS data in different formats and at different time intervals. A standard FTP client is used to access this service and the user is required to register. Another EDAS available is the Networked Transport of RTCM via Internet Protocol (NTRIP). The data available through this service is DGNSS corrections and carrier phase measurements. This service also provides messages for Real-Time Kinematic (RTK) applications [36].

The SoL service needs to provide highly accurate positioning and provide integrity data for safety-critical application areas. This service is provided mainly for aviation, however it is also widely used in maritime, railways and road application areas. This service was launched on the 2^{nd} of March 2011 by the European GNSS Agency (GSA). Alerts are noticed to the user in case the accuracy worsens, in order for the user to be able to react to degraded navigation signals without grave consequences [38].

3.2.1 EGNOS Data Access Overlay Service (EDAS)

The corrections from the EGNOS GEO satellites are available through the EDAS FTP service. This service is the EGNOS terrestrial data service for users that are authorized to the service ([36], [39]). These corrections are provided in EMS file format for every hour of the day. One line in the EMS file contains one EGNOS message. The messages are available at 1 Hz and they are broadcast at the GPS L1 frequency. The message types and their contents are listed in Table 1. The EGNOS correction messages include long and fast term corrections. Satellite position and clock corrections are considered as long term corrections. Fast term corrections are the PRCs. Ionospheric corrections given in message types 18 and 26 are important corrections together with the integrity information provided in message type 6 [40].

Table 1: Message types of EGNOS corrections provided from the EDAS FTP service [40].

Type	Contents
0	Don't use for safety applications (for SBAS testing)
1	PRN Mask assignments, set up to 51 of 210 bits
2 to 5	Fast corrections
6	Integrity information
7	Fast correction degradation factor
8	Reserved for future messages
9	GEO navigation message (X, Y, Z, time, etc.)
10	Degradation Parameters
11	Reserved for future messages
12	SBAS Network Time/UTC offset parameters
13 to 16	Reserved for future messages
17	GEO satellite almanacs
18	Ionospheric grid point masks
19 to 23	Reserved for future messages
24	Mixed fast corrections/long term satellite error corrections
25	Long term satellite error corrections
26	Ionospheric delay corrections
27	SBAS Service Message
28	Clock-Ephemeris Covariance Matrix Message
29 to 61	Reserved for future messages
62	Internal Test Message
63	Null Message

According to the EGNOS OS Definition Document [41], by applying EGNOS corrections to GPS raw data of the receiver, the errors decrease by around 2-3 m. The error sources and their magnitudes for GPS and EGNOS are shown in Figure 10. GPS SCREW stands for the Satellite Residual Error for the Worst User Location for

the residual range error caused by ephemeris and clock errors. UIVD error is the User Ionospheric Vertical Delay. UERE stands for User Equivalent Range Error which is equal to 4.2 m after EGNOS corrections for 5° elevation angle and 2.4 m after EGNOS corrections for 90° elevation angle. Important to notice in Figure 10, is that the troposhere, the GPS receiver noise and the GPS multipath are not corrected by EGNOS. Only the GPS SCREW and the ionosphere are corrected by using EGNOS. The receiver noise is receiver dependent and EGNOS is unable to correct for receiver specific errors. Multipath noise is caused by the close surroundings of the receiver, which is impossible for EGNOS to monitor. The receiver may be located in the middle of a city with a lot of multipath noise or in an open field with an excellent sky visibility and very low multipath noise. The troposphere error varies a lot and depends on the local weather conditions, which makes it challenging for EGNOS to correct for this error [41].

Error sources (1σ)	GPS - Error Size (m)	EGNOS - Error Size (m)
GPS SCREW	4.0	2.3
Ionosphere (UIVD error)	2.0 to 5.0	0.5
Troposphere (vertical)	0.1	0.1
GPS Receiver noise	0.5	0.5
GPS Multipath (45° elevation)	0.2	0.2
GPS UERE 5° elevation	7.4 to 15.6	4.2 (after EGNOS corrections)
GPS UERE 90° elevation	4.15 to 6.4	2.4 (after EGNOS corrections)

Figure 10: EGNOS and GPS stand-alone error sources [41].

Figure 11 shows the 95% Horizontal Navigation System Error (HNSE) and the 95% Vertical Navigation System Error (VNSE) for the EGNOS OS coverage area. According to this figure the HNSE (95%) at the RIMS KIR in Norway is 1.1 m and the VNSE (95%) is 2.1 m. This RIMS station is close to the northern parts of Finland. These values are assumed to be the case also in the northern parts of Finland. The RIMS station LAP has an HNSE (95%) of 0.9 m and a VNSE (95%) of 1.6 m. These values may represent also the southern parts of Finland.

The minimum accuracy of EGNOS OS over Europe is given in Table 2 for HNSE (95%) and VNSE (95%) for the Worst User Location [41]. According to the EGNOS OS document ([41]) the minimum HNSE (95%) is 3 m and the VNSE (95%) is 4 m.

There are limitations to the performance of EGNOS at northeastern latitudes of Finland close to the edge of the EGNOS coverage area. This is due to low elevation angles of EGNOS GEO satellites and low visibility. The elevation angles can be as low as 14°. It has been proven in [10], that EGNOS does not provide corrections for all satellites in view, which are close to the northeastern edge of the EGNOS coverage area. This restricts the number of corrections available and leads to a decrease in accuracy.

Results presented in Chapter 5 are chosen for two days for which the difference in latitude degrees is the largest. In this way, the performance of the EGNOS OS is investigated at different latitudes close to the edge of the EGNOS coverage area.

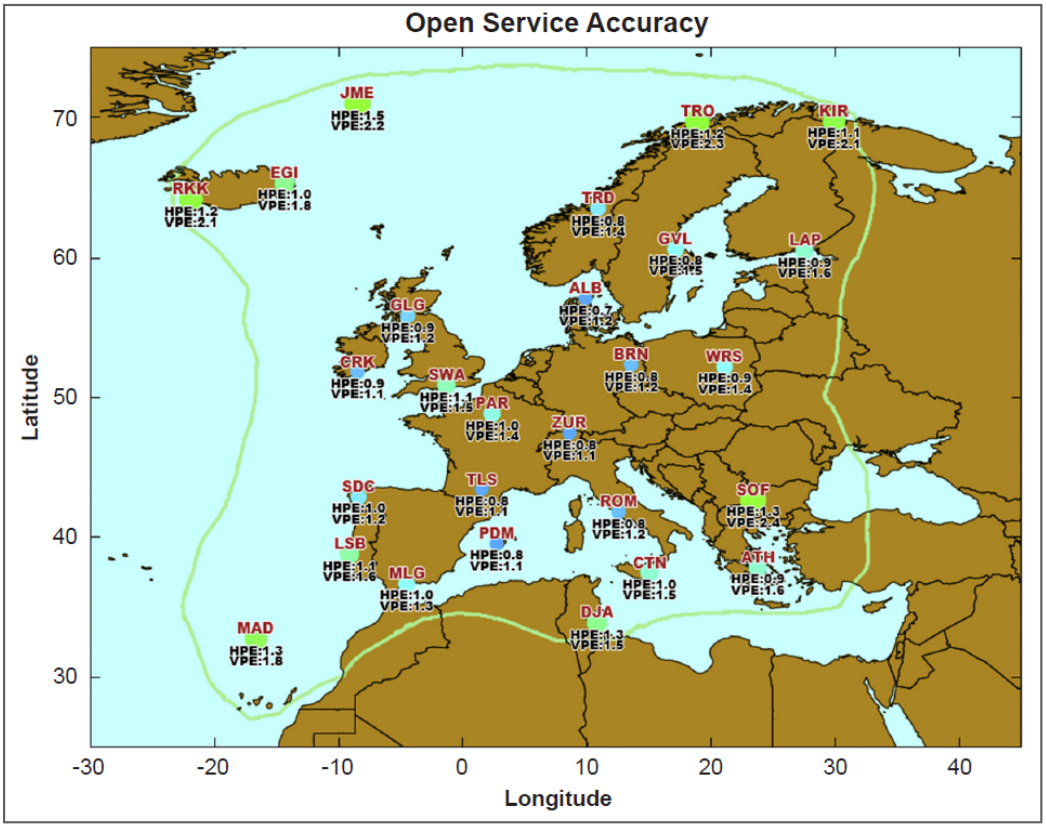

Figure 11: EGNOS OS HNSE (95%) and VNSE (95%) accuracies for the EGNOS coverage area [41].

Table 2: The HNSE (95%) and VNSE (95%) accuracies for the EGNOS OS [41].

Accuracy	**Definition**	**Value**
Horizontal	Corresponds to a 95% confidence bound of the 2-dimensional position error in the horizontal local plane for the Worst User Location	3m
Vertical	Corresponds to a 95% confidence bound of the 1-dimensional unsigned position error in the local vertical axis for the Worst User Location	4m

The goal of this thesis is to compare the LiVi DGPS and EGNOS SBAS services with respect to each other and to the GPS only solution in a real-life situation for a vessel travelling in the Baltic Sea. Chapter 4 gives a description of the test setup and how the GPS solution is augmented by using DGPS and SBAS corrections.

4 Data Collection and Analysis Tools

This chapter includes descriptions of the data collection and analysis tools. The data was collected in a test campaign as part of an international FAMOS project. The analysis tool is explained here and the governing equations used to apply the DGPS and SBAS corrections are presented here.

4.1 FAMOS Project

The Baltic Sea is a challenging sea for efficient navigation because of land uplift and the incomplete water depth mapping. Vessels need to add unnecessary safety margins because of the uncertainties in water depth levels in the Baltic Sea. These safety margins decrease the efficiency of the vessels' fuel consumption and cause an additional safety risk to the maritime traffic. Most of these challenges are solvable through accurate GNSS positioning [42]. The FAMOS project is lead by the Swedish Maritime Administration and it is co-financed by the European Union Connecting Europe Facility. This project has many collaborators from all around Europe: the Danish Geodata Agency, the Estonian Maritime Administration, the Finnish Transport Agency, the German Federal Agency for Cartography and Geodesy, the German Federal Maritime and Hydrographic Agency, the GFZ, Lantmäteriet, the Lithuanian Maritime Safety Administration, the Maritime Administration of Latvia, FGI, SSPA Sweden AB, the Swedish Meteorological and Hydrological Institute, Tallinn University of Technology and the Technical University of Denmark. At FGI the project is led by the Department of Geodesy and Geodynamics. The GNSS research is led by the Department of Navigation and Positioning [43].

4.1.1 Test Campaign

The test campaign on the research vessel Aranda of the Finnish Environment Research Institute (SYKE) in the Baltic Sea as part of the FAMOS project took place on the 5^{th}-10^{th} of June 2017. The trip of the test campaign is shown in Figure 12. This figure shows also the nine LiVi DGPS stations with their station IDs. The trip of the Aranda research vessel for this test campaign week is shown with different colored markers in Figure 12, to show where the vessel was travelling on the specific days of the test campaign. The blue markers close to Vaasa denotes the first day of the test campaign on the 5^{th} of June. The vessel continues travelling towards the northern parts of the Gulf of Bothnia on the second day of the test campaign on the 6^{th} of June, which is illustrated with the purple markers in Figure 12. Aranda travels back towards Vaasa on the third day (7^{th} of June), shown with the orange colored markers. Continuing towards the central and southern parts of the Gulf of Bothnia, on the fourth day (8^{th} of June) of the test campaign, marked by the yellow dots. The southern part of the Gulf of Bothnia is reached on the fifth day (9^{th} of June) of the test campaign, illustrated with the green markers in Figure 12. On the last day (10^{th} of June) of the test campaign, Aranda is travelling towards Helsinki, marked by the black dots in Figure 12.

The GNSS equipment of the Aranda research vessel on this trip was one NovAtel receiver, three uBlox receivers and two Septentrio receivers. The analysis given in Chapter 5 presents the data collected from the NovAtel receiver which was connected to a multi-GNSS Leica antenna. The reference for the GNSS data is the reference system composed of the NovAtel receiver and the Inertial Measurement Unit (IMU). The IMU corrects constantly the disturbances felt by the receiver and provides a very accurate position solution to the receivers.

Figure 12: The test campaign with the Aranda research vessel on the 5^{th}-10^{th} of June 2017. The red labels show the LiVi DGPS stations with their specific station IDs. The trip of Aranda is illustrated with different colored marks depending on the day of the test campaign. The blue check marks are for day 1 ($5th$ of June), the purple marks are for day 2 ($6th$ of June), the orange marks are for day 3 (7^{th} of June), the yellow marks are for day 4 (8^{th} of June), the green marks are for day 5 (9^{th} of June) and the black marks are for day 6 (10^{th} of June).

4.2 Software Analysis Tool

The data collected during the test campaign was analysed by using the FGI-GSRx software receiver in MATLAB. This multi-GNSS and multi-frequency software receiver is developed at FGI. Firstly, the binary data from the NovAtel receiver was decoded. The NovAtel binary data was decoded to a Receiver Independent Exchange Format (RINEX) version 3.02 by using the NovAtel Convert program, which is dedicated for converting NovAtel binary data to different formats. The RINEX format is a useful way to express GNSS data from different receivers. This format was developed by the Astronomical Institute of the University of Berne. The first RINEX version 1 was launched in 1989 at the 5^{th} International Geodetic Symposium on Satellite Positioning in Las Cruces, New Mexico in the U.S. [44].

After decoding the data and transforming it to track results, the navigation algorithm was run in the FGI-GSRx software for the GPS only solution. For the GPS only solution the inputs to the navigation algorithm were the RINEX navigation file from the NovAtel receiver, the track results, the reference trajectory from the IMU and the NovAtel system. The GPS only solution was run through the navigation algorithm of the FGI-GSRx software. Corrections for the SV clock, group delay differential and troposphere are included in the GPS observables. The group delay differential consists of the delay emerged from the hardware leading to the antenna and from the antenna itself, when the signal travels through these components. It is a correction factor between the L1 and L2 signals computed at the antenna phase center ([40],[45]).

The PRCs provided from the LiVi DGPS stations correct for the troposphere and ionosphere. The FGI-GSRx algorithm corrects for the missing correction parameters for the LiVi augmented solution including for the satellite clock and the group delay. Equation 8, shows how the LiVi PRC is applied to the raw PR of the receiver before this parameter is run through the navigation, namely as

$$\mathrm{PR_{i,LiVi}} = \mathrm{PR_{i,raw}} + \mathrm{PRC_{i,LiVi}} + \delta_{\mathrm{i,corr}} - \mathrm{T_{i,GD}}, \tag{8}$$

where $\mathrm{PR_{i,raw}}$ is the raw PR of the receiver, $\mathrm{PRC_{i,LiVi}}$ is the PRC from the LiVi DGPS station, $\delta_{\mathrm{i,corr}}$ stands for the clock correction factor and $\mathrm{T_{i,GD}}$ is the group delay differential between the L1 and L2 signals. The LiVi corrected PR, $\mathrm{PR_{i,LiVi}}$, is computed for every i^{th} SV.

The EGNOS augmented solution includes corrections for fast term e.g. PRCs and RRCs, and long term corrections e.g. ionosphere, troposphere, group delay and satellite clock corrections. The fast term correction is computed with the following equation

$$\mathrm{PRC_{i,EGNOS_{fast}}} = \mathrm{PRC_{i,current}} + \mathrm{RRC_{i,current}} \cdot (\mathrm{t_{rec}} - \mathrm{t_{i,current}}), \tag{9}$$

where $\mathrm{PRC_{i,current}}$ is the closest matching PRC to the time of the observable and within the timeout interval given in EGNOS message 7, according to Table 1, $\mathrm{RRC_{i,current}} = (\mathrm{PRC_{i,current}} - \mathrm{PRC_{i,previous}})/(\mathrm{t_{i,current}} - \mathrm{t_{i,previous}})$, where $\mathrm{t_{i,current}}$ is

the time of the $PRC_{i,current}$, $PRC_{i,previous}$ is the PRC which matches the closest to the time of the $PRC_{i,current}$ within half of the timeout interval and $t_{i,previous}$ is the time of the $PRC_{i,previous}$, and t_{rec} stands for the time of the observable. The $PRC_{i,EGNOS_{fast}}$ is computed for every i^{th} SV.

The long term correction is determined as

$$PRC_{i,EGNOS_{long}} = c \cdot (\Delta_{i,tsv} + \delta\Delta_{i,tsv} - T_{i,GD}) + I_{i,corr} + T_{i,corr}, \tag{10}$$

where c is the speed of light ($\approx 3 \times 10^8$ m/s), $\Delta_{i,tsv}$ is the clock correction term which includes the correction for the relativistic effect, $\delta\Delta_{i,tsv}$ stands for the clock time error estimate, $T_{i,GD}$ is the group delay differential factor, $I_{i,corr}$ is the correction factor for the ionosphere and $T_{i,corr}$ stands for the tropospheric correction factor.

Finally, the total PR corrected by EGNOS is computed by adding the fast and long term correction factors to the raw PR of the observable as

$$PR_{i,EGNOS} = PR_{i,raw} + PRC_{i,EGNOS_{fast}} + PRC_{i,EGNOS_{long}}. \tag{11}$$

Section 5.4 offers an additional DGNSS augmentation technique for the GPS signal namely an SSR error correction model. This correction model is applied to the GPS only solution by using a different software than for the two augmentation techniques described earlier. The SSR solution was obtained by using the Microsoft Visual Studio Express 2013 development tool in the C++ programming language. The algorithms included in the code are based on the work conducted in the P3 service project by FGI [46]. The SSR corrected solution includes a tropospheric correction from the Saastamoinen Zenith Hydrostatic Delay (ZHD) model and the Niell mapping function [47].

The next chapter presents the performance comparison of the satellite-based augmentation methods. Additionally, the chapter includes the validation of the software tool through a static 24-hour validation test in the FGI laboratory facility. A summary of the performance comparison concludes this chapter.

5 Performance Comparison of Augmentation Techniques

The results from the NovAtel receiver of two days of the week-long test campaign (5^{th}-10^{th} of June 2017) on the Aranda research vessel are analysed in this chapter. The first day that is analysed is the second day of the test campaign on the 6^{th} of June 2017 from 08:00:03 UTC time or 201621 s GPS TOW to 16:11:48 UTC time or 231126 s GPS TOW. The analysis covers this day of the test campaign because the Aranda research vessel is travelling in the most northern parts of the Baltic Sea. The highest latitude reached by the Aranda research vessel during this day is 65°23'2" N at 23°28'52" E longitude. This area is challenging because of the limitations of EGNOS corrections at northern latitudes and the low visibility of satellites at these latitudes. This area falls inside the EGNOS OS coverage area shown in Figure 11. The Marjaniemi station is chosen for the LiVi DGPS corrections because it is located the closest to the Aranda research vessel on this day. The EGNOS corrections used on this day are taken from the EGNOS PRN 136 GEO satellite.

The other day that is analysed is the fifth day of the test campaign, on the 9^{th} of June 2017 from 07:00:03 UTC time or 457221 s GPS TOW to 15:07:08 UTC time or 486446 s GPS TOW. This day of the test campaign was chosen because the Aranda research vessel is travelling in the southern parts of the Baltic Sea. The southern most latitude reached during this day is 59°43'47" N and at 20°23'47" E longitude. The LiVi DGPS corrections for this day is used from the Turku station because it is located the closest to the Aranda research vessel on this day. The EGNOS corrections used are from the EGNOS PRN 123 GEO satellite.

The difference in latitude between the northern most measurement and the southern most measurement of the test campaign is 5°41'13". The reference system used on both days of the analysis is the IMU and the NovAtel receiver system. The statistical analysis of the results are composed of different variables computed with the FGI-GSRx software receiver. The GPS only solution is corrected for the SV clock, group delay differential and troposphere. The relations given below are used to compute the statistical values presented in Tables 3-5, 7-8. It is common to use a Local-Level Frame (ENU) in satellite-based navigation when comparing the accuracies of different solutions.

The horizontal deviation is computed by using the following equation

$$\text{horizontal}_{\text{deviation}} = \sqrt{\text{E}^2 + \text{N}^2}, \tag{12}$$

where E stands for the 'East' component and N stands for the 'North' component.

The vertical deviation is computed by taking the absolute of the Up component vector as

$$\text{vertical}_{\text{deviation}} = \mid \text{U} \mid, \tag{13}$$

where U stands for the 'Up' component.

HNSE (95%) is computed by

$$\text{index}_{\text{hor}} = \lfloor \text{n}_{\text{hor}} \cdot 0.95 \rfloor, \tag{14}$$

where n_{hor} stands for the length of the $\text{horizontal}_{\text{deviation}}$ sorted in ascending order and

$$\text{HNSE}(95\%) = \text{horizontal}_{\text{deviation}_{\text{sort}}}(\text{index}_{\text{hor}}). \tag{15}$$

VNSE (95%) is computed by

$$\text{index}_{\text{ver}} = \lfloor \text{n}_{\text{ver}} \cdot 0.95 \rfloor, \tag{16}$$

where n_{ver} stands for the length of the $\text{vertical}_{\text{deviation}}$ sorted in ascending order and

$$\text{VNSE}(95\%) = \text{vertical}_{\text{deviation}_{\text{sort}}}(\text{index}_{\text{ver}}). \tag{17}$$

The Root Mean Square Error (RMSE) in the East direction (RMSE_{E}) is computed by using the following equation

$$\text{RMSE}_{\text{E}} = \sqrt{\frac{\sum_{i=1}^{\text{n}}([\text{E}_1, \text{E}_2, ...\text{E}_\text{n}]^2)}{\text{n}}}, \tag{18}$$

where $[\text{E}_1, \text{E}_2, ...\text{E}_\text{n}]$ is the column vector of the East component error of the data with length n.

The RMSE in the North direction (RMSE_{N}) is computed by using the following equation

$$\text{RMSE}_{\text{N}} = \sqrt{\frac{\sum_{i=1}^{\text{n}}([\text{N}_1, \text{N}_2, ...\text{N}_\text{n}]^2)}{\text{n}}}, \tag{19}$$

where $[\text{N}_1, \text{N}_2, ...\text{N}_\text{n}]$ is the column vector of the North component error of the data with length n.

The RMSE in the Up direction (RMSE_{U}) is computed by using the following equation

$$\text{RMSE}_{\text{U}} = \sqrt{\frac{\sum_{i=1}^{\text{n}}([\text{U}_1, \text{U}_2, ...\text{U}_\text{n}])^2)}{\text{n}}}, \tag{20}$$

where $[\text{U}_1, \text{U}_2, ...\text{U}_\text{n}]$ is the column vector of the Up component error of the data with length n.

The RMSE Horizontal ($RMSE_H$) is computed by using the following equation

$$RMSE_H = \sqrt{{RMSE_E}^2 + {RMSE_N}^2}. \tag{21}$$

The RMSE Vertical ($RMSE_V$) is computed by

$$RMSE_V = \sqrt{{RMSE_U}^2}. \tag{22}$$

The RMSE 3-D ($RMSE_{3D}$) is calculated by using the following relation

$$RMSE_{3D} = \sqrt{{RMSE_E}^2 + {RMSE_N}^2 + {RMSE_U}^2}. \tag{23}$$

The following section provides a validation of how the augmented techniques are applied to the GPS only solution. An about 24-hour validation test was conducted in the laboratory facility of FGI at 60°10'40" N latitude and at 24°33'44" E longitude on the 7^{th}-8^{th} of January 2019. The statistical analysis and figures support the validation of these techniques.

5.1 Validation of the Analysis Tool

The capabilities of EGNOS and LiVi to correct the GPS only solution are validated in this section. Data was logged for about 24 hours in a static condition by using the NovAtel receiver. The physical location of the validation test was at the FGI laboratory facility and using the GNSS antenna Antcom located on the roof of the FGI building at 60°10'40" N latitude and at 24°33'44" E longitude. The roof is an ideal location for the GNSS antenna, because of the open sky location allowing for more GPS signals to reach the antenna and minimizing multipath effects. The long duration of the validation test proves the ideal capabilities of EGNOS and LiVi corrections to augment the GPS signal. The LiVi Porkkala DGPS station provided corrections for this data. The EGNOS corrections provided by the EGNOS PRN 123 GEO satellite are used here. Table 3 lists the statistical values of the GPS only solution, LiVi DGPS and EGNOS corrected solutions. Figure 13 illustrates the ground plots for GPS, LiVi and EGNOS solutions in the North East coordinate plane. Figure 14 provides the plots for the three solutions in the Up component with respect to GPS TOW. Figure 15 shows the horizontal deviation and the number of satellites used in the navigation for the three solutions. The last figure, Figure 16, gives the vertical deviation as a function of time for all three solutions.

In Table 3 a positive (+) improvement denotes an improvement and a negative (−) improvement denotes a decrease, not an improvement, with respect to GPS. By inspecting the results given in Table 3, it is concluded that the EGNOS corrected solution improves the GPS only solution by 22.63% in HNSE (95%) and by 27.98% in VNSE (95%). The HNSE (95%) and the VNSE (95%) are both within the requirements of the EGNOS OS stated in Table 2.

The LiVi DGPS corrections improve the GPS only solution by 24.98% in HNSE (95%) and by 39.37% in VNSE (95%). The requirements of the LiVi DGPS service are also met because the accuracy is less than 10 m 95% of the time. However, the

Table 3: Validation test of the NovAtel receiver on the 7^{th} of January 2019 at 12:08:52 UTC time or 130150 s GPS TOW to the 8^{th} of January 2019 at 12:08:52 UTC time or 216550 s GPS TOW. Statistical values provided for the GPS only solution, LiVi (Porkkala station) and EGNOS (PRN 123) corrected solutions.

Validation 7.-8.1.2019			
	GPS	GPS + LiVi	GPS + EGNOS
HNSE (95%) [m]	2.89	2.16	2.23
VNSE (95%) [m]	4.60	2.79	3.31
$RMSE_H$ [m]	1.71	1.15	1.36
$RMSE_V$ [m]	2.74	1.42	1.84
$RMSE_{3D}$ [m]	3.23	1.83	2.28
Horizontal deviation mean [m]	1.53	0.94	1.17
Vertical deviation mean [m]	2.39	1.04	1.46
No. satellites used mean	9.34	8.99	7.56
No. Epochs	87088	86399	86347
HNSE (95%) improvement with respect to GPS [%]		+24.98	+22.63
VNSE (95%) improvement with respect to GPS [%]		+39.37	+27.98

requirement of the LiVi DGPS service accuracy in practise of less than 2 m 95% of the time is not met.

The largest improvements in both horizontal and vertical directions are obtained by LiVi. However, the difference between LiVi and EGNOS in the horizontal direction is only around 2%. In the vertical direction the difference is more significant namely about 11%.

Both of the augmented solutions improve the GPS only solution of the NovAtel receiver in a static condition for 24 hours which means that the method is validated of augmenting the GPS solution.

The following section gives the results of the second day of the test campaign.

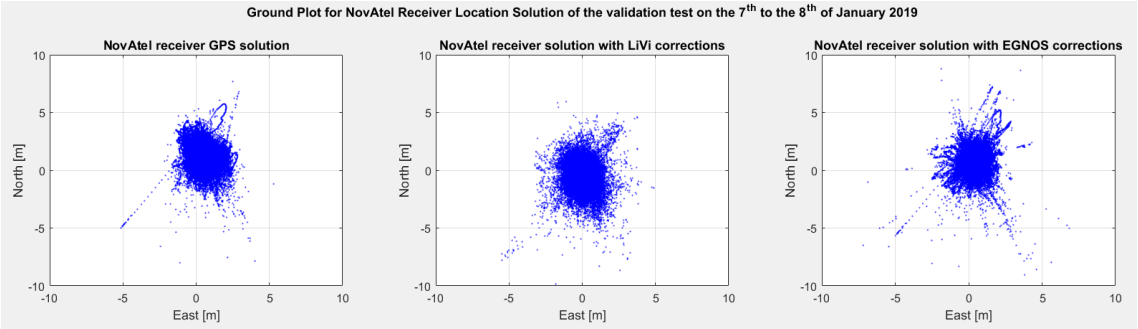

Figure 13: Ground plots in the North East coordinate plane for GPS, GPS+LiVi and GPS+EGNOS for the validation test from the 7^{th} of January 2019 at 12:08:52 UTC time or 130150 s GPS TOW to 8^{th} of January 2019 at 12:08:52 UTC time or 216550 s GPS TOW for the NovAtel receiver. The leftmost figure gives the GPS only solution, the middle figure shows the GPS+LiVi augmented solution and the rightmost figure is the GPS+EGNOS augmented solution.

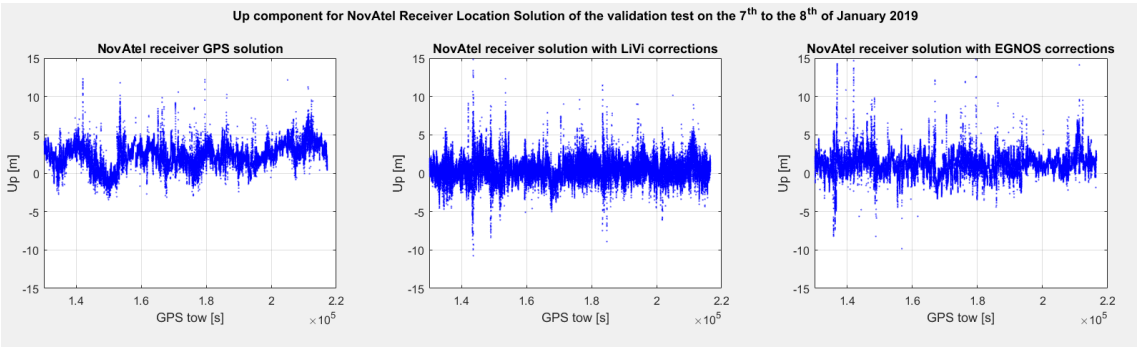

Figure 14: Up component for GPS, GPS+LiVi and GPS+EGNOS for the validation test from the 7^{th} of January 2019 at 12:08:52 UTC time or 130150 s GPS TOW to 8^{th} of January 2019 at 12:08:52 UTC time or 216550 s GPS TOW for the NovAtel receiver. The leftmost figure gives the GPS only solution, the middle figure shows the GPS+LiVi augmented solution and the rightmost figure is the GPS+EGNOS augmented solution.

5.2 Second Day of the Test Campaign

This section presents the results of the second day of the test campaign for the NovAtel receiver. Statistical values have been computed by using the relations presented in the beginning of this chapter. These values are listed in Table 4 for the GPS only solution and the two augmented solutions LiVi and EGNOS. For all solutions the ground plot, Up component, horizontal deviation with number of satellites used in the navigation and the vertical deviation are illustrated graphically.

On the second day of the test campaign on the 6^{th} of June 2017 at 08:00:03 UTC time or 201621 s GPS TOW, the Aranda research vessel was located according to the IMU+NovAtel system at 65°23'01.4" N and 23°27'46.5" E. The trajectory of this day of the test campaign is illustrated in Figure 12 by the purple colored markers. The

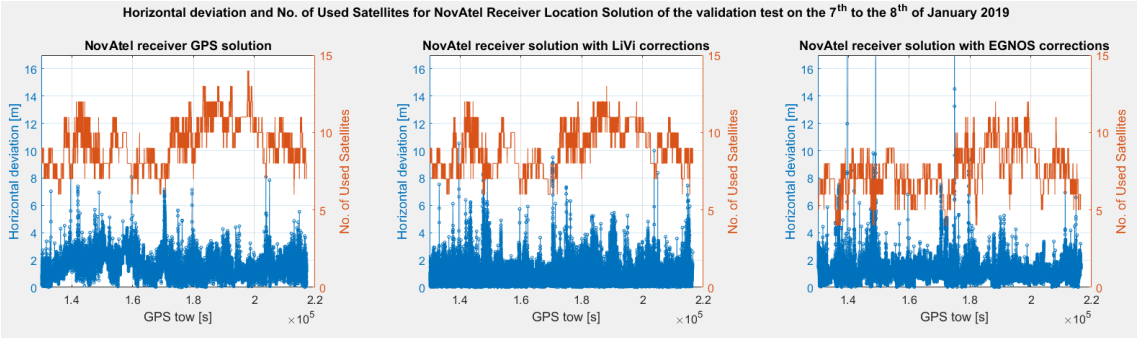

Figure 15: Horizontal deviation and number of satellites used for GPS, GPS+LiVi and GPS+EGNOS for the validation test from the 7^{th} of January 2019 at 12:08:52 UTC time or 130150 s GPS TOW to 8^{th} of January 2019 at 12:08:52 UTC time or 216550 s GPS TOW for the NovAtel receiver. The blue lines give the horizontal deviation and the orange lines the number of satellites used. The leftmost figure gives the GPS only solution, the middle figure shows the GPS+LiVi augmented solution and the rightmost figure is the GPS+EGNOS augmented solution.

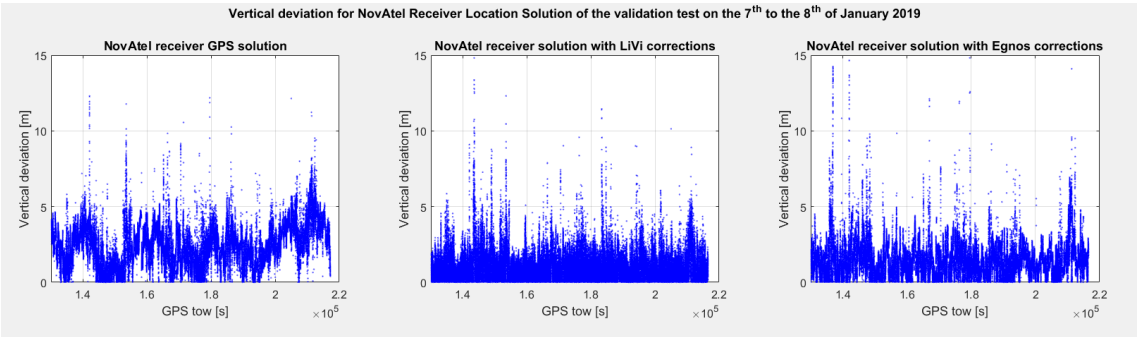

Figure 16: Vertical deviation for GPS, GPS+LiVi and GPS+EGNOS for the validation test from the 7^{th} of January 2019 at 12:08:52 UTC time or 130150 s GPS TOW to 8^{th} of January 2019 at 12:08:52 UTC time or 216550 s GPS TOW for the NovAtel receiver. The leftmost figure gives the GPS only solution, the middle figure shows the GPS+LiVi augmented solution and the rightmost figure is the GPS+EGNOS augmented solution.

northern most location of this day of the test campaign was at 65°23'2" N latitude and 23°28'52" E longitude. The data set analysed for this day of the test campaign is from 08:00:03 UTC time or 201621 s GPS TOW to 16:11:48 UTC time or 231126 s GPS TOW.

The LiVi augmented solution is composed of PRCs obtained from the Marjaniemi DGPS station, which is located closest to the vessel on this day. The EGNOS corrections broadcast from the EGNOS PRN 136 GEO satellite are used for this data set. The results are presented in this section for the GPS only solution, LiVi and EGNOS augmented solutions.

The ground plots in the North East coordinate plane are shown in Figure 17.

The leftmost figure is the GPS only solution, the figure in the middle is the LiVi Marjaniemi augmented solution and the rightmost figure is the EGNOS PRN 136 corrected solution. The same position for each solution is illustrated throughout Figures 17-20. The vertical Up coordinate solution is presented in Figure 18. The horizontal deviations for all solutions are shown in Figure 19 as the blue colored lines. In this figure, the number of satellites used in the navigation solution is shown with orange colored lines. This gives an overview of the reasons behind the sudden increase in horizontal deviation when the number of satellites used drops. The peaks in the horizontal deviation correlates with a decrease in the number of satellites used in the navigation. Finally, in Figure 20, the vertical deviations are shown for all three solutions.

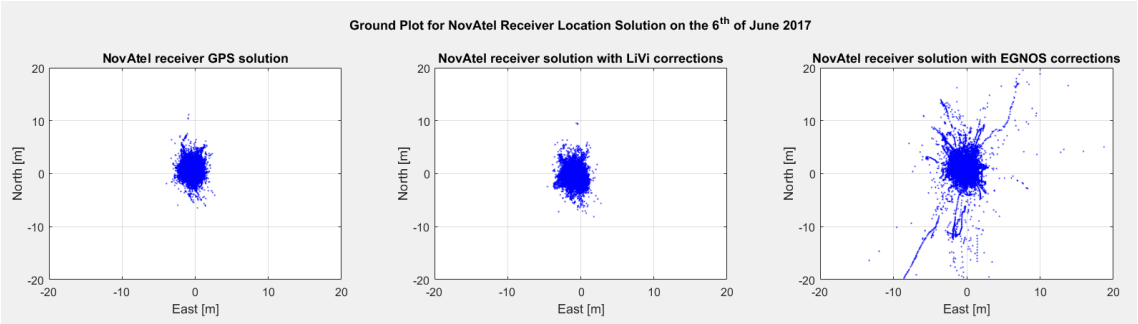

Figure 17: Ground plots in the North East coordinate plane for GPS, GPS+LiVi and GPS+EGNOS on day 2 of testing on the 6^{th} of June 2017 from 08:00:03 UTC time or 201621 s GPS TOW to 16:11:48 UTC time or 231126 s GPS TOW for the NovAtel receiver. The leftmost figure gives the GPS only solution, the middle figure shows the GPS+LiVi augmented solution and the rightmost figure is the GPS+EGNOS augmented solution.

The ground plot in Figure 17 for the EGNOS corrected solution is the least precise solution compared to the two other solutions. Multiple outliers are visible in the plot which make the solution less precise. However, most of the data points in the EGNOS solution are centered around the (0,0) point. The GPS solution and the LiVi corrected solution look similar to each other and it is difficult to conclude only based on these plots which one is more precise or accurate.

Table 4 gives the HNSE (95%) and VNSE (95%) values for all three solutions, which were computed by using the equations presented in the beginning of this chapter in Equations 12-17. GPS only performs the best in HNSE (95%) compared to the two other augmented solutions. The last two columns in the table give the improvement with respect to GPS in HNSE (95%) and VNSE (95%). The EGNOS solution increases HNSE (95%) with respect to GPS by 102.72%. The limitations of EGNOS at northern latitudes can explain this result. However in VNSE (95%) the EGNOS solution improves the GPS solution by 18.44%. The LiVi solution performs better than EGNOS for this data set, even though it worsens the GPS solution in HNSE (95%) by 6.60% but in VNSE (95%) the improvement is as significant as 41.46%.

Table 4: Day 2 of the test campaign on the 6^{th} of June 2017 from 08:00:03 UTC time or 201621 s GPS TOW to 16:11:48 UTC time or 231126 s GPS TOW. Statistical values provided for the GPS only solution, LiVi (Marjaniemi station) and EGNOS (PRN 136) corrected solutions.

	Day 2: 6^{th} of June 2017		
	GPS	GPS + LiVi	GPS + EGNOS
HNSE (95%) [m]	2.77	2.96	5.62
VNSE (95%) [m]	9.38	5.49	7.65
$RMSE_H$ [m]	1.57	1.81	3.37
$RMSE_V$ [m]	6.25	2.70	4.78
$RMSE_{3D}$ [m]	6.44	3.25	5.85
Horizontal deviation mean [m]	1.34	1.63	2.08
Vertical deviation mean [m]	5.85	2.07	2.69
No. satellites used mean	10.63	9.98	6.43
No. Epochs	29506	29506	29506
HNSE (95%) improvement with respect to GPS [%]		−6.60	−102.72
VNSE (95%) improvement with respect to to GPS [%]		+41.46	+18.44

$RMSE_H$, $RMSE_V$ and $RMSE_{3D}$ are also given in Table 4. These parameters were computed by using Equations 18-23. By inspecting the $RMSE_H$ values it is clear that the GPS solution is the most accurate. In $RMSE_V$ the LiVi provides the most accurate solution and the GPS solution the worse. In $RMSE_{3D}$ the best result is again obtained with LiVi and the worse with GPS only.

The mean values of the horizontal and vertical deviations are also given in the table together with the mean value of the number of satellites used. The GPS only solution has the best horizontal deviation performance and EGNOS has the worse performance in this direction. In vertical deviation the most accurate solution is provided by LiVi. This is also visible from Figure 20, where it can be seen that the

GPS only solution has a higher vertical deviation than the other two solutions. The EGNOS solution has peaks in the data at times when the number of satellites drops. An important observation to make is that the number of satellites used in average is the lowest for the EGNOS augmented solution, with only 6.43 satellites on average. This is a fairly low value which explains the poor performance of EGNOS OS at high northern latitudes. A decrease in the number of satellites used, which is illustrated in Figure 19, translates to an increase in horizontal deviation. These are related to each other, which means that the less satellites available for the navigation algorithm the higher becomes the deviation.

In Figure 18, the Up components are plotted with respect to the GPS TOW. In the EGNOS plot on the far right, there are peaks in the Up component which can be explained by the decrease in the number of satellites at that time of the measurements shown in Figure 19. By inspecting these two figures it can be seen that EGNOS performs poorly because of high fluctuations in the data. GPS only and LiVi plots have much less fluctuations or peaks in their data compared to the EGNOS solution. The same can be observed from Figure 20, which illustrates the vertical deviations for all three solutions. The vertical deviation is also plotted with respect to GPS TOW. The GPS only solution shows a higher vertical deviation compared to the two augmented solutions. There is an offset from the zero axis in the GPS solution. This offset disappears when corrections are applied by LiVi or EGNOS.

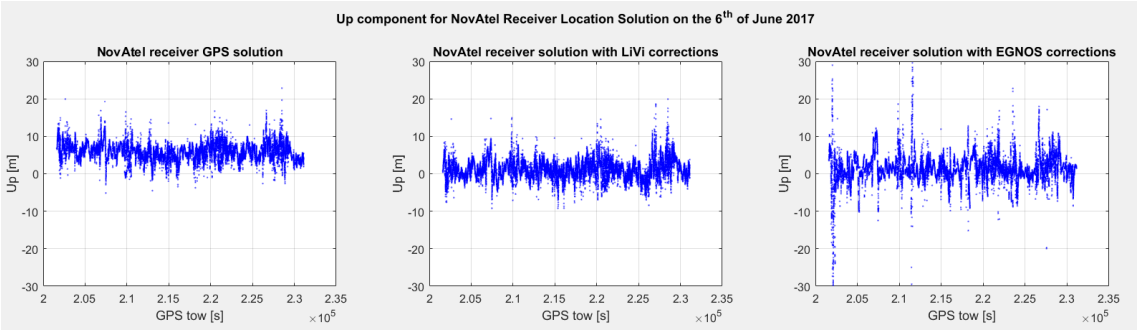

Figure 18: Up component for GPS, GPS+LiVi and GPS+EGNOS on day 2 of testing on the 6^{th} of June 2017 from 08:00:03 UTC time or 201621 s GPS TOW to 16:11:48 UTC time or 231126 s GPS TOW for the NovAtel receiver. The leftmost figure gives the GPS only solution, the middle figure shows the GPS+LiVi augmented solution and the rightmost figure is the GPS+EGNOS augmented solution.

5.3 Fifth Day of the Test Campaign

The analysis of the fifth day of the test campaign on the 9^{th} of June 2017 is analysed from 07:00:03 UTC time or 457221 s GPS TOW to 15:07:08 UTC time or 486446 s GPS TOW. During this day the Aranda research vessel was located in the most southern parts of the test campaign at a minimum latitude of 59°43'47" N and 20°23'47" E longitude. The Aranda research vessel was located in the beginning

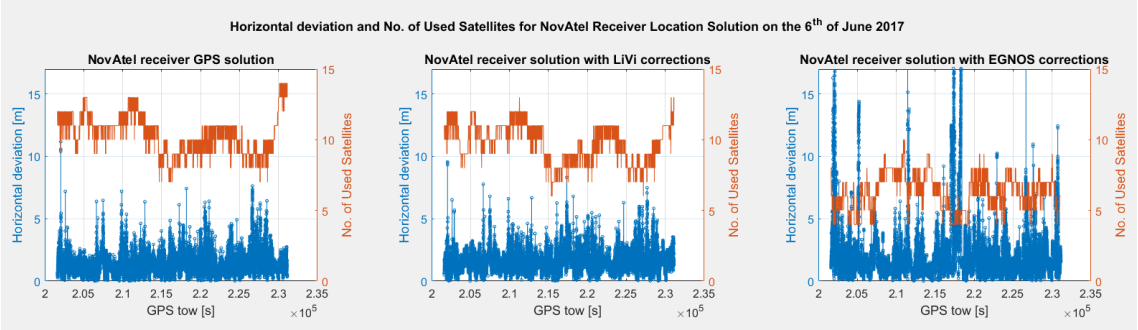

Figure 19: Horizontal deviation and number of satellites used for GPS, GPS+LiVi and GPS+EGNOS on day 2 of testing on the 6^{th} of June 2017 from 08:00:03 UTC time or 201621 s GPS TOW to 16:11:48 UTC time or 231126 s GPS TOW for the NovAtel receiver. The blue lines give the horizontal deviation and the orange lines the number of satellites used. The leftmost figure gives the GPS only solution, the middle figure shows the GPS+LiVi augmented solution and the rightmost figure is the GPS+EGNOS augmented solution.

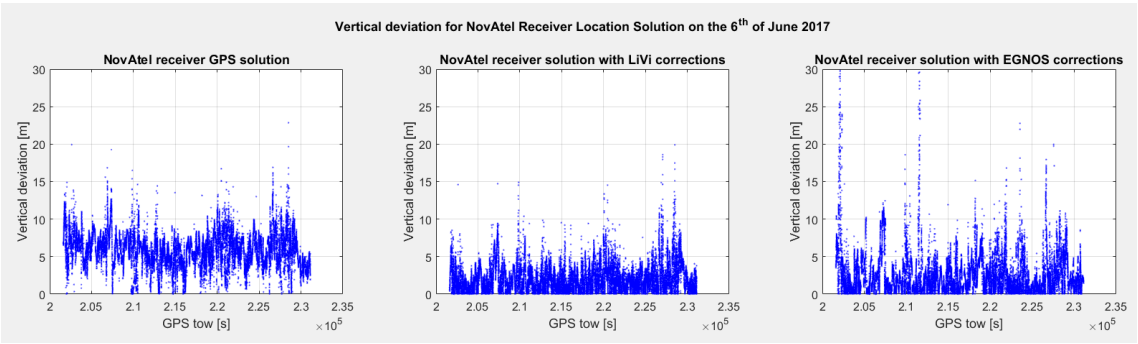

Figure 20: Vertical deviation for GPS, GPS+LiVi and GPS+EGNOS on day 2 of testing on the 6^{th} of June 2017 from 08:00:03 UTC time or 201621 s GPS TOW to 16:11:48 UTC time or 231126 s GPS TOW. The leftmost figure gives the GPS only solution, the middle figure shows the GPS+LiVi augmented solution and the rightmost figure is the GPS+EGNOS augmented solution.

of this day according to the IMU+NovAtel system at 60°11'20.7" N latitude and 19°08'32.5" E longitude. The trajectory of this day is illustrated in Figure 12 shown with the green colored markers. The data analysed here is from the NovAtel receiver for a GPS only solution and two augmented solutions by LiVi and EGNOS. The same set of plots as for day 2 are provided for this day in Figures 21-24. The DGPS station chosen for this data set is Turku because it was the closest LiVi DGPS station on this day. The EGNOS corrections broadcast from the EGNOS PRN 123 GEO satellite are used for this data set.

By comparing the three ground plots in Figure 21, it is seen that the LiVi and EGNOS corrected solutions have some fluctuations in the North East coordinate directions, deviating a bit from the (0,0) point. The GPS solution seems more precise and accurate in this coordinate plane compared to the two augmented solutions.

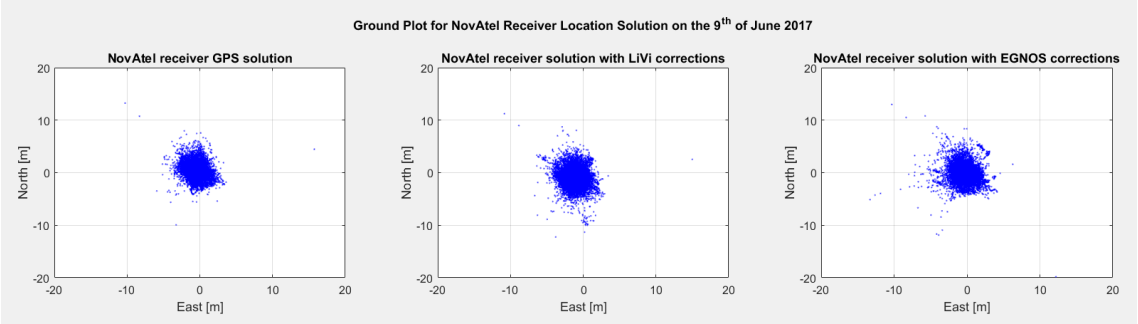

Figure 21: Ground plots in the North East coordinate plane for GPS, GPS+LiVi and GPS+EGNOS on day 5 of testing on the 9^{th} of June 2017 from 07:00:03 UTC time or 457221 s GPS TOW to 15:07:08 UTC time or 486446 s GPS TOW for the NovAtel receiver. The leftmost figure gives the GPS only solution, the middle figure shows the GPS+LiVi augmented solution and the rightmost figure is the GPS+EGNOS augmented solution.

Table 5 gives the statistical values for the data set for these three different solutions. The same variables are given for this data set as for the previous data sets in Tables 3-4. The GPS only solution performs the best in the horizontal direction. In HNSE (95%) the LiVi solution makes the GPS only solution less accurate by 30.25% and the EGNOS solution gives a 15.23% decrease in accuracy compared to GPS. Additionally, the $\mathrm{RMSE_H}$ value and the horizontal deviation mean value are the lowest for the GPS only solution.

The largest improvement of the augmented solutions compared to GPS occurs in the vertical direction. The LiVi corrected solution improves the GPS solution by 46.44% in VNSE (95%) and the EGNOS corrected solution improves the same parameter by 47.06%. The vertical deviation mean value is the lowest for the LiVi corrected solution and the difference with respect to EGNOS is 12 cm. The LiVi solution has the lowest $\mathrm{RMSE_V}$ value compared to GPS and EGNOS. In $\mathrm{RMSE_{3D}}$ EGNOS performs the best with an accuracy of 3.13 m, compared to the GPS only solution of 6.74 m. This is a significant improvement for both augmented solutions compared to the GPS only solution.

The GPS solution has the highest mean value of 10.21 satellites used in the navigation on average compared with the other two solutions. The LiVi corrected solution has the second highest number of satellites used with 9.59 satellites on average and EGNOS has the lowest number of satellites used with 8.16 satellites. However, this is a significant improvement for EGNOS compared to day 2 when the average number of satellites used was only 6.43. On day 5 both the accuracy and availability of EGNOS improve significantly compared to day 2.

The Up component with respect to GPS TOW for all three solutions is shown in Figure 22. The GPS only solution has an offset from the zero axis and deviates the most compared to the two other solutions. This offset disappears when corrections are applied from LiVi and EGNOS.

In horizontal direction the GPS only solution performs the best, which can also

Table 5: Day 5 of the test campaign on the 9^{th} of June 2017 from 07:00:03 UTC time or 457221 s GPS TOW to 15:07:08 UTC time or 486446 s GPS TOW. Statistical values provided for the GPS only solution, LiVi (Turku station) and EGNOS (PRN 123) corrected solutions.

	Day 5: 9^{th} of June 2017		
	GPS	GPS + LiVi	GPS + EGNOS
HNSE (95%) [m]	2.81	3.66	3.24
VNSE (95%) [m]	9.62	5.15	5.09
$RMSE_H$ [m]	1.61	2.22	1.71
$RMSE_V$ [m]	6.55	2.54	2.63
$RMSE_{3D}$ [m]	6.74	3.38	3.13
Horizontal deviation mean [m]	1.39	1.99	1.40
Vertical deviation mean [m]	6.18	1.93	2.05
No. satellites used mean	10.21	9.59	8.16
No. Epochs	29226	29226	29226
HNSE (95%) improvement with respect to GPS [%]		−30.25	−15.23
VNSE (95%) improvement with respect to to GPS [%]		+46.44	+47.06

be concluded from the statistics shown in Table 5. However, there are less peaks in general in the horizontal deviation for the two augmented solutions compared to day 2 of the test campaign in Figure 19. The number of satellites used in the navigation algorithm for EGNOS is much higher for this day than for day 2 which is clearly seen in Figure 23, by the orange lines. The descents in the number of satellites used cause an increase in the horizontal deviation. This is seen in Figure 23 by the correlation between a descent in the number of satellites and a sudden peak or increase in the horizontal deviation.

Figure 24 shows the vertical deviation as a function of GPS TOW for all three solutions. The GPS only solution differs the most from the zero axis compared to

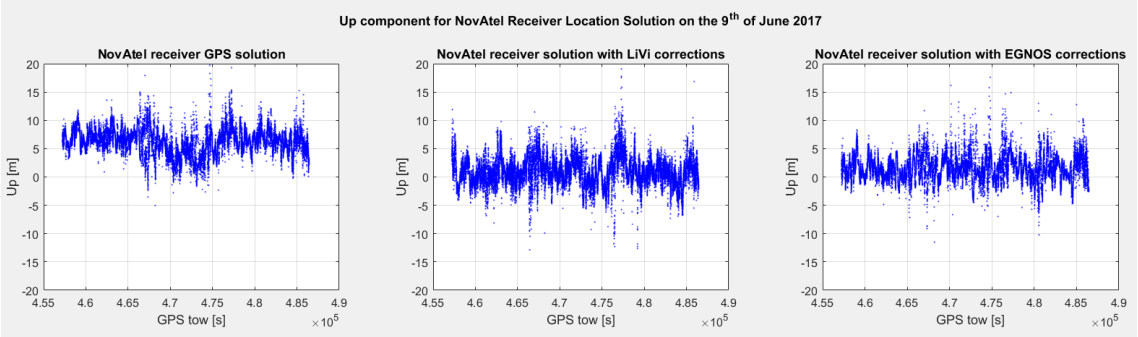

Figure 22: Up component for GPS, GPS+LiVi and GPS+EGNOS on day 5 of testing on the 9^{th} of June 2017 from 07:00:03 UTC time or 457221 s GPS TOW to 15:07:08 UTC time or 486446 s GPS TOW for the NovAtel receiver. The leftmost figure gives the GPS only solution, the middle figure shows the GPS+LiVi augmented solution and the rightmost figure is the GPS+EGNOS augmented solution.

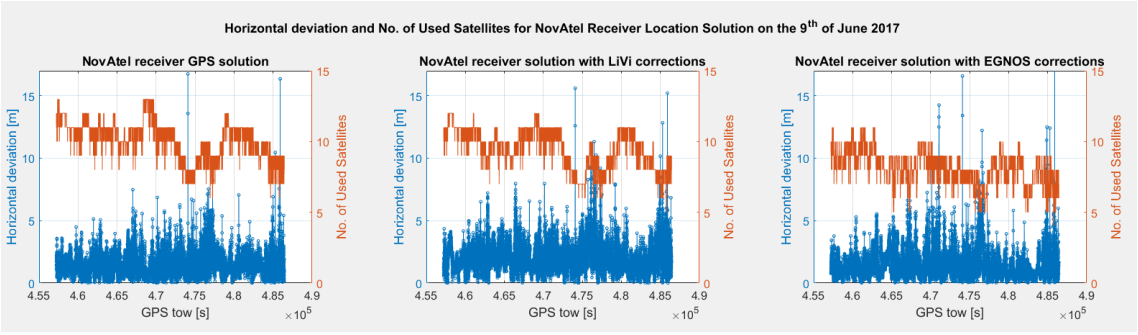

Figure 23: Horizontal deviation and number of satellites used for GPS, GPS+LiVi and GPS+EGNOS on day 5 of testing on the 9^{th} of June 2017 from 07:00:03 UTC time or 457221 s GPS TOW to 15:07:08 UTC time or 486446 s GPS TOW for the NovAtel receiver. The blue lines give the horizontal deviation and the orange lines the number of satellites used. The leftmost figure gives the GPS only solution, the middle figure shows the GPS+LiVi augmented solution and the rightmost figure is the GPS+EGNOS augmented solution.

the two augmented solutions. The same observation was made in Figure 22. The augmented solutions have a similar behaviour compared to each other. Although according to Table 5, the LiVi solution has a 12 cm lower vertical deviation compared to the EGNOS corrected solution on average.

5.4 State Space Representation (SSR)

An additional DGNSS augmentation technique is given here namely the SSR error correction model. This technique provides a Precise Point Positioning (PPP) solution to the user. The messages required to apply the SSR correction model are obtained from the FinnRef network, which is managed by FGI. The network is accessible for civilian use and it is funded by the Finnish government. FinnRef has broadcast

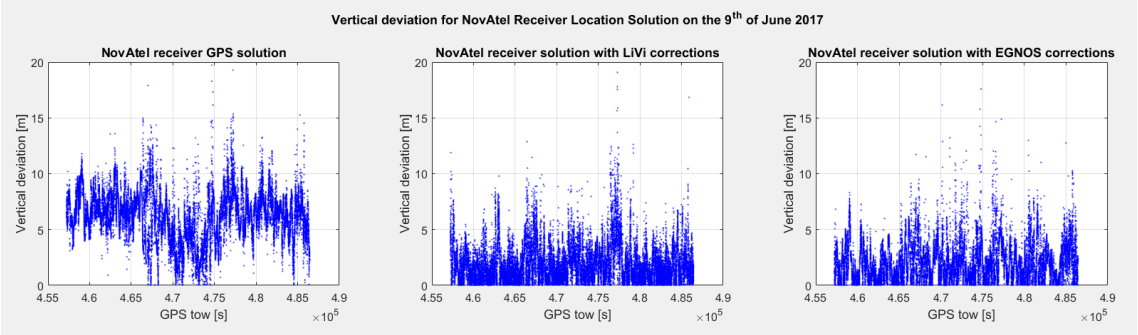

Figure 24: Vertical deviation for GPS, GPS+LiVi and GPS+EGNOS on day 5 of testing on the 9^{th} of June 2017 from 07:00:03 UTC time or 457221 s GPS TOW to 15:07:08 UTC time or 486446 s GPS TOW. The leftmost figure gives the GPS only solution, the middle figure shows the GPS+LiVi augmented solution and the rightmost figure is the GPS+EGNOS augmented solution.

SSR correction messages since 2014. The SSR messages broadcast by FinnRef are RTCM standardised, apart from two messages. Table 6 lists the content of the SSR messages broadcast by the FinnRef network. The messages starting with the Id number 10 are RTCM standardised and the messages starting with the Id number 12 are not yet RTCM standardised. Message 4090 is a proprietary message. According to Table 6, the SSR messages 1057 to 1059 provide GPS orbit, clock and satellite code bias correction information. Messages 1264 and 1265, which are not yet RTCM standardised provide, corrections for the ionosphere Vertical Total Electron Content (VTEC) spherical harmonics and GPS satellite phase bias. The proprietary message number 4090 offers ionosphere Slant Total Electron Content (STEC) polynomial corrections [47].

Table 6: RTCM SSR messages content [47]

RTCM Message Id	**Content**
1057	SSR GPS Orbit Correction Message
1058	SSR GPS Clock Correction Message
1059	SSR GPS Satellite Code Bias Message
1264	SSR Ionosphere VTEC Spherical Harmonics Message
1265	SSR GPS Satellite Phase Bias Message
Proprietary 4090	SSR Ionosphere STEC Polynomial Message

The SSR corrections were applied by using the software tool described in Section 4.2. The GPS only solution from day 2 of the test campaign is augmented by SSR corrections. The statistical values for the SSR corrected solution are given in Table 7. The same parameters are provided here as in Tables 3-5. In addition, Table 7 lists the statistical parameters for the LiVi and EGNOS corrected solutions for day 2 of the test campaign. In this way, it is easier to compare all augmented solutions with respect to the GPS solution and with respect to each other.

The HNSE (95%) and $RMSE_H$ values of the SSR solution are almost identical to the LiVi augmented solution. In HNSE (95%) the SSR solution decreases the accuracy compared to the GPS solution by 6.70%. The LiVi solution decreases the accuracy of GPS by 6.60%. The VNSE (95%) of the SSR corrected solution is also close to the LiVi augmented solution. The SSR augmentation improves the GPS only solution by 42.97% where the LiVi solution improves GPS by 41.46%. The number of satellites used by SSR is slightly lower than for the LiVi solution, namely 8.20 satellites used on average.

The $RMSE_V$ value for SSR is closer to the EGNOS augmented solution than to the LiVi solution. The SSR solution is 18 cm more accurate than EGNOS, however it is almost 2 m less accurate than the LiVi augmentation. In $RMSE_{3D}$ the SSR solution is the second most accurate compared to the other solutions. The horizontal deviation mean value for the SSR solution is however the most accurate compared to the other solutions. The vertical deviation mean value is as accurate as 2.16 m, improving the GPS only solution by 3.69 m.

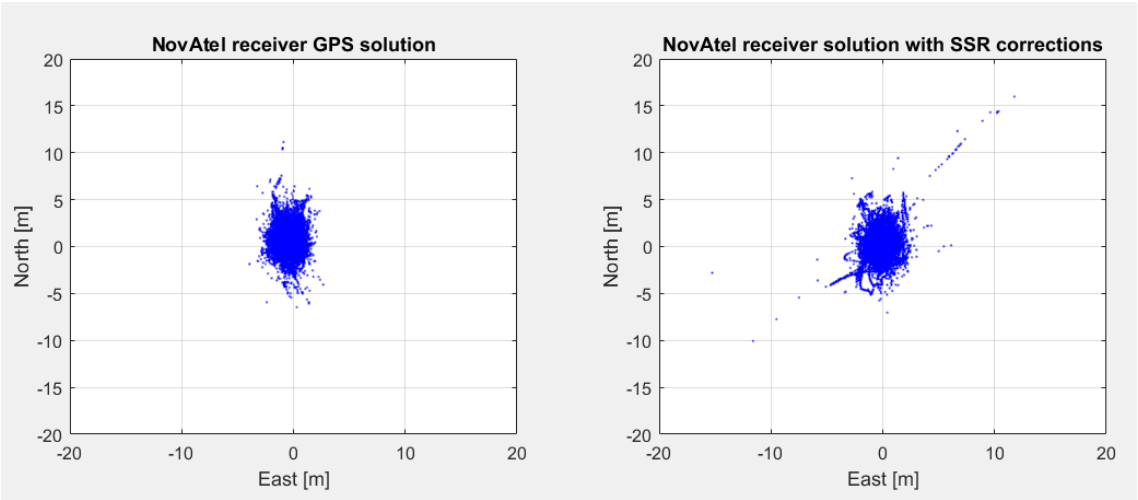

Figure 25: Ground plots in the North East coordinate plane for GPS and GPS+SSR on day 2 of testing on the 6^{th} of June 2017 from 08:00:03 UTC time or 201621 s GPS TOW to 16:11:48 UTC time or 231126 s GPS TOW for the NovAtel receiver. The leftmost figure gives the GPS only solution and the rightmost figure is the GPS+SSR corrected solution.

Figure 25 illustrates the ground plots of the GPS only solution and the SSR corrected solution. The SSR solution is more centered around the (0,0) point compared to the GPS solution. However there are some outliers in the SSR solution which are not present in the GPS solution. Figure 26 shows the Up component with respect to GPS TOW for the GPS only and the SSR corrected solutions. The Up components for the GPS only solution are higher compared to the SSR corrected solution, which means that the SSR solution is more accurate in the Up component. The data points are fluctuating more closely around zero, with some peaks present. The horizontal deviation of the two solutions are illustrated side by side in Figure 27. The number of satellites used is also shown in the same plots. The SSR solution has

Table 7: Statistical values for GPS only solution, SSR, LiVi (Marjaniemi station) and EGNOS (PRN 136) corrected solutions for the NovAtel receiver on day 2 of the test campaign on the 6^{th} of June 2017 from 08:00:03 UTC time or 201621 s GPS TOW to 16:11:48 UTC time or 231126 s GPS TOW.

	Day 2: 6^{th} of June 2017			
	GPS	GPS + SSR	GPS + LiVi	GPS + EGNOS
HNSE (95%) [m]	2.77	2.96	2.96	5.62
VNSE (95%) [m]	9.38	5.35	5.49	7.65
$RMSE_H$ [m]	1.57	1.80	1.81	3.37
$RMSE_V$ [m]	6.25	4.60	2.70	4.78
$RMSE_{3D}$ [m]	6.44	4.94	3.25	5.85
Horizontal deviation mean [m]	1.34	1.27	1.63	2.08
Vertical deviation mean [m]	5.85	2.16	2.07	2.69
No. satellites used mean	10.63	8.20	9.98	6.43
No. Epochs	29506	29506	29506	29506
HNSE (95%) improvement with respect to GPS [%]		−6.70	−6.60	−102.72
VNSE (95%) improvement with respect to GPS [%]		+42.97	+41.46	+18.44

a few deviating peaks in the data at times when the number of satellites decreases. The same behaviour is less obvious for the GPS only solution, which shows a more stable behaviour in the horizontal deviation when the number of satellites decreases. Finally, Figure 28 gives the vertical deviations as a function of GPS TOW for the two solutions. The same trend is seen here as in Figure 26, the vertical deviation is much higher for the GPS only solution compared to the SSR augmented solution. There are some higher peaks included in the data set of the SSR solution, which are not as high for the GPS only solution. These peaks are formed due to the discontinuance of the SSR corrections. Overall, the GPS solution becomes significantly better after applying SSR corrections.

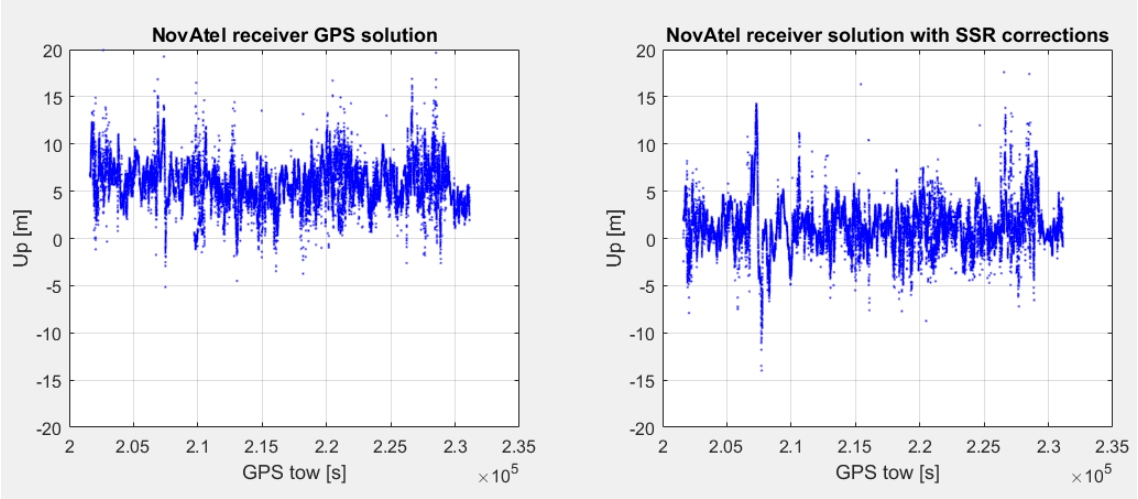

Figure 26: Up component for GPS and GPS+SSR on day 2 of testing on the 6^{th} of June 2017 from 08:00:03 UTC time or 201621 s GPS TOW to 16:11:48 UTC time or 231126 s GPS TOW for the NovAtel receiver. The leftmost figure gives the GPS only solution and the rightmost figure is the GPS+SSR corrected solution.

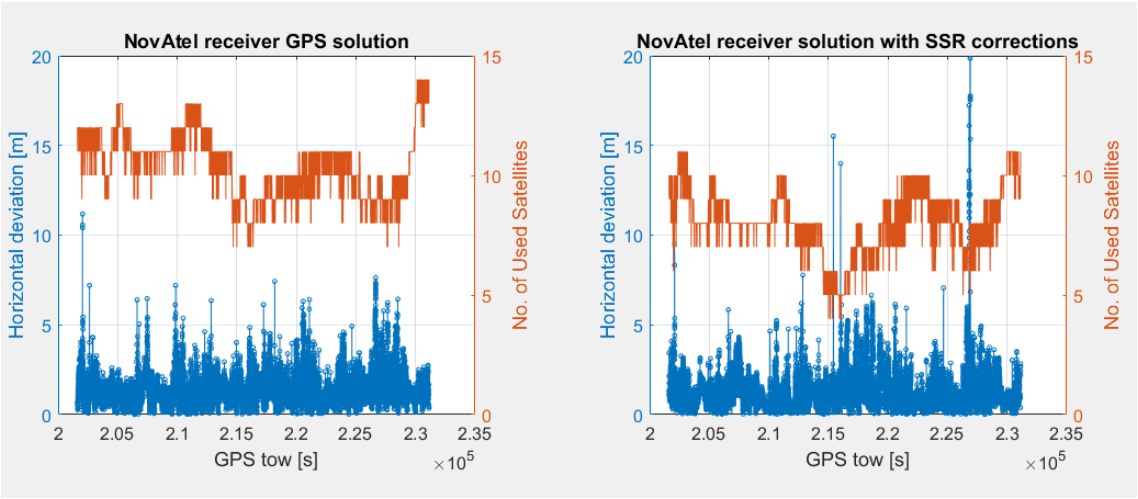

Figure 27: Horizontal deviation and number of satellites used for GPS and GPS+SSR on day 2 of testing on the 6^{th} of June 2017 from 08:00:03 UTC time or 201621 s GPS TOW to 16:11:48 UTC time or 231126 s GPS TOW for the NovAtel receiver. The blue lines give the horizontal deviation and the orange lines the number of satellites used. The leftmost figure gives the GPS only solution and the rightmost figure is the GPS+SSR corrected solution.

5.5 Summary of the Performance Comparison

The performance comparison are based on two days of the test campaign. One day where the Aranda research vessel was located at the most northern region and one day where it was travelling in the most southern region of the test campaign. The northern most latitude reached on day 2 of the test campaign was at 65°23'2" N

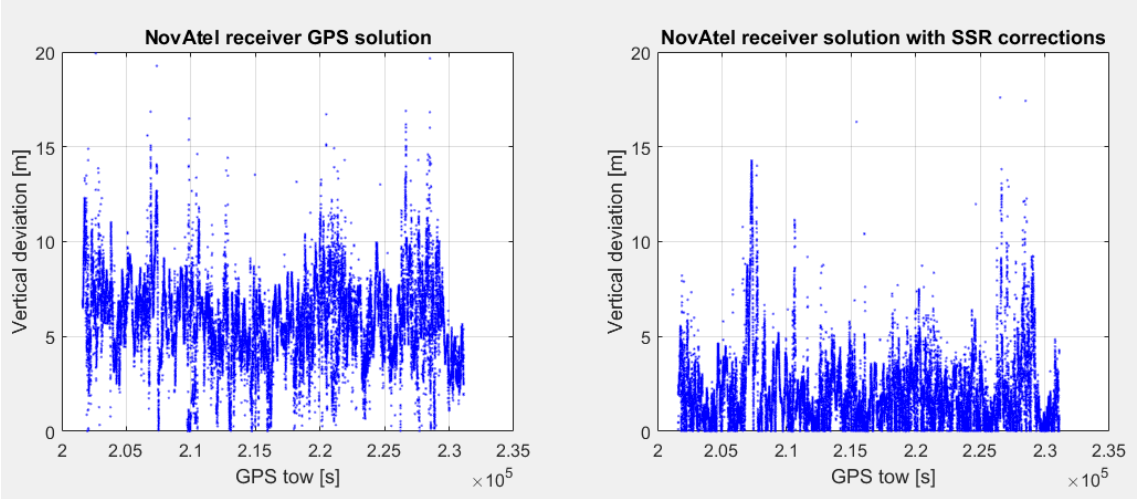

Figure 28: Vertical deviation for GPS and GPS+SSR on day 2 of testing on the 6^{th} of June 2017 from 08:00:03 UTC time or 201621 s GPS TOW to 16:11:48 UTC time or 231126 s GPS TOW. The leftmost figure gives the GPS only solution and the rightmost figure is the GPS+SSR corrected solution.

and the southern most latitude was 59°43'47" N reached on day 5. The difference between these two days in latitude degrees is 5°41'13". This difference has shown to have an impact on the accuracy and the availability of EGNOS corrections. This was an expected result given the limitations of the EGNOS OS at northern latitudes close to the edge of the EGNOS coverage area.

The EGNOS OS promises a horizontal accuracy of less than 3 m and a vertical accuracy of less than 4 m with a 95% confidence bound, which was given in Table 2 in Section 3.2.1. On day 2 of the test campaign neither of these two requirements are met for the EGNOS service. The HNSE (95%) of EGNOS on day 5 of the test campaign improves compared to day 2, although failing to meet the requirement of EGNOS OS. The vertical requirement is also not met on day 5 of the test campaign for the EGNOS augmented solution. As it was mentioned in Section 3.1.1, the LiVi DGPS service ensures an accuracy of less than 10 m 95% of the time, and in practice an accuracy between 1 to 2 m for its users. The statistical parameters for the two days of the test campaign show that the LiVi service provides less than 10 m accuracy 95% of the time for both days. However, the 1-2 m accuracy requirement in practice is not met on either of these two days.

Table 8 lists the HNSE (95%), VNSE (95%) and the average of satellites used of all three solutions for both days of the test campaign. The improvements with respect to GPS are also given for HNSE (95%) and VNSE (95%). In HNSE (95%) the GPS only solution performs better than the augmented solutions for both days. This means that the augmentation methods are not so efficient in decreasing the GPS signal errors in the horizontal direction. The EGNOS solution worsens the GPS only solution the most for day 2 of the test campaign. However, on day 5 the EGNOS solution performs better than LiVi in HNSE (95%). In VNSE (95%) on day 2, LiVi gave the highest improvement with respect to GPS compared to EGNOS,

Table 8: Summary of the results for GPS only, GPS+LiVi and GPS+EGNOS solutions for the NovAtel receiver on day 2 and 5 of the test campaign.

	Day 2			Day 5		
	GPS	GPS + LiVi	GPS + EGNOS	GPS	GPS + LiVi	GPS + EGNOS
HNSE (95%) [m]	2.77	2.96	5.62	2.81	3.66	3.24
VNSE (95%) [m]	9.38	5.49	7.65	9.62	5.15	5.09
No. satellites used mean	10.63	9.98	6.43	10.21	9.59	8.16
HNSE (95%) improvement with respect to GPS [%]		−6.60	−102.72		−30.25	−15.23
VNSE (95%) improvement with respect to GPS [%]		+41.46	+18.44		+46.44	+47.06

with an improvement of 41.46%. On day 5 the highest improvement in VNSE (95%) was offered by EGNOS, with an improvement of 47.06%.

The GPS only solution uses on average more satellites than the two augmentation techniques. It also showed a more stable behaviour in horizontal deviation when the number of satellites used dropped. The augmented solutions showed higher deviations in the horizontal direction when the number of satellites decreased, illustrated in Figures 19 and 23.

There are clear differences between the performance of day 2 and day 5 for the EGNOS augmented solution. The number of satellites used increases from 6.43 satellites on average to 8.16 satellites used when the latitude changes by 5°41'13" towards the south. The increased number of satellites used means that there are more corrections available for the satellites in view. This improves the accuracy of the navigation solution. From decreasing the HNSE (95%) by 102.72% on day 2, the EGNOS augmented solution decreases the HNSE (95%) of the GPS solution by 15.23% on day 5. In VNSE (95%) the EGNOS solution improved the GPS only solution by 18.44% on day 2 and on day 5 by a significant 47.06%.

The LiVi augmented solution performs in a similar way on both days. The changes in latitude does not affect the performance of LiVi. The LiVi DGPS stations cover the entire Baltic Sea region and offer corrections without disruptions. The stations are located close to the sea to be able to cover the entire Finnish watercourse. The number of satellites used are almost the same on average for both days. The HNSE (95%) however worsens on day 5 from decreasing the GPS solution by 6.60% on day 2 to 30.25% on day 5. A possible reason for this decrease in horizontal accuracy may

be because of an increased distance between the vessel and the DGPS station. On day 2 the vessel was more closely located to the Marjaniemi DGPS station compared to day 5 when the closest station was the Turku DGPS station. When the distance between the receiver and the DGPS station increases, the DGPS corrections do not give a close representation of the atmospheric effects at the receiver location. This is a possible explanation to the decrease in horizontal accuracy between these two days of the LiVi DGPS service. On day 5 LiVi provides an improvement of 46.44% in VNSE (95%) compared to the 41.46% improvement on day 2 with respect to GPS.

The SSR augmented solution, shown in Section 5.4, came close to the performance level of the LiVi corrected solution on day 2 of the test campaign. The slightly decreased number of satellites used for SSR compared to LiVi increased the $RMSE_{3D}$ and $RMSE_V$ values of SSR. However, the HNSE (95%) and VNSE (95%) values were almost the same for the SSR and the LiVi corrected solutions on day 2. An SSR corrected solution provides an accurate and highly improving solution for the maritime sector even at northern latitudes. LiVi and SSR can work as compensation techniques for the EGNOS corrections at northern latitudes. These two techniques could offer a more reliable and continuous correction service to the GPS signal in the maritime sector close to the edge of the EGNOS coverage area.

6 Conclusion

The research question was to compare the performance of DGPS and SBAS augmented techniques in a real-life situation for a vessel travelling in the Baltic Sea. The anomalies in the sea level, the lack of a common geodetic vertical reference level to GNSS coordinates and the heavy maritime traffic are only a few challenges that are faced in this region. The low elevation angles and visibility of GNSS satellites at northern latitudes are additional challenges in this region. The research question was answered through a thorough accuracy analysis given in Chapter 5. The data was collected during a week-long test campaign from the 5^{th}-10^{th} of June 2017 on board the research vessel Aranda in the Baltic Sea. The test campaign was also a part of the activities in the international project FAMOS. The accuracy, availability and reliability of GPS correction services were analysed for two days of the test campaign. On the second day, 6^{th} of June 2017, the data logging started at 08:00:03 UTC time or 201621 s GPS TOW and ended at 16:11:48 UTC time or 231126 s GPS TOW. The Aranda research vessel travelled on this day in the northernmost parts of the Gulf of Bothnia at 65°23'2" N latitude and 23°28'52" E longitude. On the fifth day, 9^{th} of June 2017, the data logging started at 07:00:03 UTC time or 457221 s GPS TOW and ended at 15:07:08 UTC time or 486446 s GPS TOW. The Aranda research vessel travelled on this day in the southernmost parts of the test campaign at 59°43'47" N latitude and 20°23'47" E longitude.

EGNOS corrections show a large difference in the performance between north and south Baltic Sea regions. Results show that EGNOS corrections give a lower accuracy in the northern latitudes compared to the southern latitudes. The vessel was located on day 2 in the northern most parts of the test campaign close to the EGNOS coverage area's edge. In this region, EGNOS provided corrections for fewer satellites than in the south Baltic Sea region on day 5. Whenever satellites are not within the EGNOS coverage area the service does not provide corrections for them. This excludes potential GPS signals from the receiver's navigation solution which decreases the accuracy. Another observation made from the results was that whenever the number of satellites in view dropped the horizontal deviation increased. The large peaks in the horizontal deviation were aligned with the valleys of the number of satellites used in the navigation solution. The EGNOS OS performance requirements in both horizontal and vertical directions were not met on either of the two days.

LiVi corrections do not show a similar drop in the performance as EGNOS in north Baltic Sea regions compared to the southern regions. The accuracy of LiVi corrections depends on the distance between the receiver and the DGPS station. On day 5 there was a decrease in horizontal accuracy because of the increased distance between the vessel and the DGPS station compared to day 2. The Turku DGPS station which was used on day 5 has a 50 km smaller coverage area compared to the Marjaniemi DGPS station used on day 2. An increased distance between the user and the DGPS station leads to a bad representation of the atmospheric effects of the user's location. As a result the accuracy of the corrected navigation solution becomes less accurate. Apart from the decreased accuracy in the horizontal direction, the

vertical accuracy improved on day 5 compared to day 2. The LiVi DGPS service provides PRCs for all satellites in view on both days. The number of satellites used in the navigation solution by LiVi is almost the same as for GPS. The LiVi service requirement of less than 10 m 95% of the time are met on both days. However, the requirement in practice of 1-2 m 95% of the time is not met on either of the two days.

An additional DGNSS augmentation technique was presented in this thesis, namely an SSR error correction model provided by the FinnRef network managed by FGI. The SSR performance on day 2 reached closely to the performance level of LiVi in horizontal and vertical directions. The number of satellites used in the navigation by SSR was lower by around one satellite on average compared to LiVi, however the vertical accuracy of SSR was slightly better compared to LiVi. The accuracy of SSR corrections are in both horizontal and vertical directions significantly better compared to EGNOS on day 2. SSR provides an accurate and continuous augmentation of the GPS signal for maritime applications in north Baltic Sea regions.

The performance of different augmentation techniques in the Baltic Sea were evaluated in this thesis. Recommendations for achieving safer maritime navigation were also made based on the analysis of the collected data. The augmentation techniques provide an improvement to GPS in the vertical direction on both days of the test campaign. These techniques are able to give an accurate navigation solution for users in the Baltic Sea. Maritime navigation becomes more safe and precise by applying augmentation corrections to the GPS signal. EGNOS shows decays in the horizontal and vertical accuracies in north Baltic Sea regions. The limitations of EGNOS at northern latitudes exist close to the edge of the EGNOS coverage area. The availability of EGNOS corrections is significantly decreased in this region. LiVi performs similarly on both days, however an increased distance between the receiver and the DGPS station decreases the accuracy in the horizontal direction. The availability of LiVi corrections is constant in both north and south Baltic Sea regions. The SSR corrections can be considered as an alternative to EGNOS in north Baltic Sea regions after it is fully RTCM standardized. Including carrier phase data will enhance the accuracy considerably compared to the code data which was analysed here. The performance comparison in this thesis proves that the augmentation techniques strengthen the GPS signal in maritime navigation.

References

[1] Porretta, M., Banos, D. J., Crisci, M. et al. *GNSS Evolutions for Maritime - An Incremental Approach. InsideGNSS,* May-June 2016, Journal Online. pp. 54–62. Accessed on 8.8.2018. Available: http://insidegnss.com/auto/mayjune16-WP.pdf.

[2] Ekman, M. *The Changing Level of the Baltic Sea during 300 Years: A clue to Understanding the Earth.* Åland Islands, Summer Institute for Historical Geophysics, 2009.

[3] Desai, S. D. Observing the pole tide with satellite altimetry. *Journal of Geophysical Research (Oceans),* 2002, Journal Paper, vol. 107, no. C11, pp. 1–13.

[4] International Maritime Organization (IMO). Introduction to IMO. Document Online. Updated 2018. Accessed on 29.8.2018. Available: http://www.imo.org/en/About/Pages/Default.aspx.

[5] European Global Navigation Satellite Systems Agency (GSA). GNSS Market Report, 2015, issue 4, pp. 47–55. Luxembourg, Publications Office of the European Union. DOI:10.2878/251572.

[6] International Maritime Organization (IMO). Guidance for private maritime security companies and passenger ship recommendations agreed by IMO's Maritime Safety Committee. *Maritime Safety Committee (MSC) 90th session 16 to 25 May 2012,* Committee Session Paper Online. Updated 2012. Accessed on 29.8.2018. Available: http://www.imo.org/en/MediaCentre/MeetingSummaries/MSC/Pages/MSC-90th-session.aspx.

[7] International Maritime Organization (IMO). Meeting Summary. *Maritime Safety Committee (MSC) 95th session 3-12 June 2015,* Committee Session Paper Online. Updated 2015. Accessed on 29.8.2018. Available: http://www.imo.org/en/MediaCentre/MeetingSummaries/MSC/Pages/MSC-95th-session.aspx.

[8] International Maritime Organization (IMO). Meeting Summary. *Sub-Committee on Navigation, Communications and Search and Rescue (NCSR) 4th session 6-10 March 2017,* Committee Session Paper Online. Updated 2017. Accessed on 29.8.2018. Available: http://www.imo.org/en/MediaCentre/MeetingSummaries/NCSR/Pages/NCSR-4th-session.aspx.

[9] The National Coordination Office for Space-Based Positioning Navigation and Timing & National Oceanic and Atmospheric Administration (NOAA). Selective Availability. Document Online. Updated 23.9.2016. Accessed on 9.8.2018. Available: https://www.gps.gov/systems/gps/modernization/sa/.

[10] Bhuiyan, M. Z. H. et al. EGNOS in Northeastern Europe - How well does it perform? *GPS World,* pp. 42–48, 2017.

[11] Kaplan, E. D., Hegarty, C. J. *Understanding GPS: Principles and Applications.* Second Edition. Massachusetts, Artech House, 2006.

[12] United States Naval Observatory (USNO). Current GPS Constellation. Document Online. Updated 2018. Accessed on 10.5.2018. Available: http://tycho.usno.navy.mil/gpscurr.html.

[13] United States Naval Observatory (USNO). GPS Constellation Status. Document Online. Updated 9.5.2018. Accessed on 10.5.2018. Available: ftp://tycho.usno.navy.mil/pub/gps/gpstd.txt.

[14] Mallette, L., Rochat, P., White, J. An Introduction to Satellite Based Atomic Frequency Standards. *IEEE Aerospace Conference Proceedings, IEEE Xplore,* 2008, Conference Proceedings. pp. 1–9.

[15] The National Coordination Office for Space-Based Positioning Navigation and Timing & National Oceanic and Atmospheric Administration (NOAA). Space Segment. Document Online. Updated 2017. Accessed on 10.5.2018. Available: http://www.gps.gov/systems/gps/space/.

[16] European Space Agency (ESA). GPS Space Segment. Document Online. Updated 18.5.2016. Accessed on 10.5.2018. Available: http://www.navipedia.net/index.php/GPS_Space_Segment.

[17] The National Coordination Office for Space-Based Positioning Navigation and Timing & National Oceanic and Atmospheric Administration (NOAA). GPS/WAAS Program Update - Baska GNSS Conference. Conference Presentation. Updated 7.5.2018. Accessed on 9.8.2018. Available: https://www.gps.gov/multimedia/presentations/2018/05/baska/auerbach.pdf.

[18] Time Service Dept U.S. Naval Observatory Washington DC. Leap Seconds. Document Online. Updated 7.1.2002. Accessed on 7.8.2018. Available: https://tycho.usno.navy.mil/leapsec.html.

[19] NovAtel Inc. Unit Conversions. Document Online. Updated 8.8.2018. Accessed on 8.8.2018. Available: https://www.novatel.com/support/knowledge-and-learning/published-papers-and-documents/unit-conversions/.

[20] Naval Postgraduate School (NPS) Department of Oceanography. Time Systems and Dates - GPS Time. Document Online. Updated 5.6.2017. Accessed on 7.8.2018. Available: http://www.oc.nps.edu/oc2902w/gps/timsys.html.

[21] The National Coordination Office for Space-Based Positioning Navigation and Timing & National Oceanic and Atmospheric Administration (NOAA). Control Segment. Document Online. Updated 3.11.2017. Accessed on 8.8.2018. Available: https://www.gps.gov/systems/gps/control/.

[22] Van Sickle, J. GEOG 862: GPS and GNSS for Geospatial Professionals - Lesson 1: The GPS Signal. The Pennsylvania State University. Document Online. Updated 2018. Accessed on 9.8.2018. Available: https://www.e-education.psu.edu/geog862/book/export/html/1407.

[23] The National Coordination Office for Space-Based Positioning Navigation and Timing & National Oceanic and Atmospheric Administration (NOAA). New Civil Signals. Document Online. Updated 12.6.2017. Accessed on 9.8.2018. Available: https://www.gps.gov/systems/gps/modernization/civilsignals/.

[24] Love, A. W. GPS, atomic clocks and relativity. *IEEE Potentials,* 1994, Journal Paper, vol. 13, no. 2, pp. 11–15.

[25] Leva, J. An Alternative Closed-Form Solution to the GPS Pseudo-Range Equations. *IEEE Transactions on Aerospace and Electronic Systems,* 1996, Journal Paper, vol. 32, no. 4, pp. 1430–1439.

[26] Liikennevirasto. Radionavigointipalvelut. Document Online. Updated 2017. Accessed on 28.8.2018. Available: http://www.liikennevirasto.fi/ammattimerenkulku/liikkuminen-vesivaylilla/radionavigaatiopalvelut.

[27] Liikennevirasto. Tiedonantoja merenkulkijoille. Document Online. Updated 2018. Accessed on 7.5.2018. Available: https://www.liikennevirasto.fi/documents/20473/24074/tm_info_suomi.pdf/4d041bcb-c12d-4c90-aed1-1978a062fe2d.

[28] Liikennevirasto. Meriliikennekeskus. Document Online. Updated 2018. Accessed on 7.5.2018. Available: https://www.laivakuvat.com/meriliikennekeskus/.

[29] Radio Technical Commission for Maritime Services (RTCM). About RTCM. Document Online. Updated 2018. Accessed on 23.8.2018. Available: http://www.rtcm.org/about.html.

[30] Radio Technical Commission for Maritime Services (RTCM). RTCM Standard 10401.2 for Differential NAVSTAR GPS Reference Stations and Integrity Monitors (RSIM). RTCM Paper 221-2006-SC104-STD, vol. 1.2, 2006.

[31] Borre, K. et al. *A Software-Defined GPS and Galileo Receiver: A Single-Frequency Approach,* Massachusetts, Birkhäuser Basel, 2007.

[32] European Global Navigation Satellite Systems Agency (GSA). What is SBAS? Document Online. Updated 22.8.2018. Accessed on 22.8.2018. Available: https://www.gsa.europa.eu/european-gnss/what-gnss/what-sbas.

[33] European Space Agency (ESA). EGNOS: European Geostationary Navigation Overlay Service - Europe's first contribution to satellite navigation.

Document Online. Updated 2009. Accessed on 22.8.2018. Available: http://www.egnos-pro.esa.int/Publications/ESA_EGNOS_br284_2009.pdf.

[34] European Global Navigation Satellite Systems Agency (GSA). EGNOS System. Document Online. Updated on 16.8.2016. Accessed on 22.8.2018. Available: https://www.gsa.europa.eu/european-gnss/egnos/egnos-system.

[35] Inmarsat. About us. Document Online. Updated 2013. Accessed on 23.8.2018. Available: https://www.inmarsat.com/about-us/.

[36] European Global Navigation Satellite Systems Agency (GSA). About EDAS. Document Online. Updated 14.8.2018. Accessed on 23.8.2018. Available: https://egnos-user-support.essp-sas.eu/new_egnos_ops/services/about-edas.

[37] International Telecommunications Union (ITU). Introduction to ASN.1. Document Online. Updated 2018. Accessed on 23.8.2018. Available: https://www.itu.int/en/ITU-T/asn1/Pages/introduction.aspx.

[38] European Global Navigation Satellite Systems Agency (GSA). About SoL. Document Online. Updated 14.8.2018. Accessed on 23.8.2018. Available: https://egnos-user-support.essp-sas.eu/new_egnos_ops/services/about-sol.

[39] European Satellite Services Provider (ESSP SAS). EDAS FTP Service User Information Package Version: 1.3. ESSP SAS, 2016.

[40] Radio Technical Commission for Aeronautics (RTCA) Inc. Minimum Operational Performance Standards for Global Positioning System / Wide Area Augmentation System Airborne Equipment - RTCA DO-229D. SC-159 RTCA Inc. Washington, DC, USA, 2006.

[41] European Commission. EGNOS Open Service - Service Definition Document Revision 2.0, European Commission, Directorate-General for Enterprise and Industry, 2013.

[42] FAMOS Consortium. Activity 2: Vessel navigation for the future. Document Online. Updated 2014-2018. Accessed on 24.8.2018. Available: http://www.famosproject.eu/activities/future-navigation/.

[43] FAMOS Consortium. Project consortium. Document Online. Updated 2014-2018. Accessed on 28.10.2018. Available: http://www.famosproject.eu/famos/consortium/.

[44] Gurtner, W., Estey, L. RINEX - The Receiver Independent Exchange Format - Version 3.02 - International GNSS Service (IGS), RINEX Working Group and Radio Technical Commission for Maritime Services Special Committee 104 (RTCM-SC104). Astronomical Institute of the University of Bern, Switzerland and UNAVCO, Boulder, Colorado, USA, 2013.

[45] NAVSTAR Global Positioning System. Interface Specification, IS-GPS-200. Revision D. IRN-200D-001. El Segundo, California, USA, 2006.

[46] Finnish Geospatial Research Institute (FGI), National Land Survey of Finland (NLS). Development of a Mobile Public Precise Positioning Service Based on the National GNSS Network (P3-Service). Document Online. Updated 2018. Accessed on 19.1.2019. Available: https://p3-service.net/.

[47] Finnish Geospatial Research Institute (FGI), National Land Survey of Finland (NLS). Development of a Mobile Public Precise Positioning Service Based on the National GNSS Network (P3-Service), P3-Service Project Final Report, version 6, 2016.